Masterarbeit

verfasst von

Stefan Fürtbauer

eingereicht am

Institut für Bodenmechanik und Grundbau

der Technischen Universität Graz

Thema der Masterarbeit

Numerical Modelling of Interface Grouting Pressure

Begutachter: AO.Univ.-Prof. Dipl.-Ing. Dr.techn. M.Sc. tit. Univ.-Prof. Helmut Schweiger

Betreuer: Univ.-Ass. Dipl.-Ing. Franz Tschuchnigg

Graz, im Jänner 2012

Erklärung

Ich erkläre an Eides Statt, dass ich die vorliegende Arbeit selbstständig und ohne fremde Hilfe verfasst, andere als die angegebenen Quellen nicht benutzt und die den benutzten Quellen wörtlich und inhaltlich entnommenen Stellen als solche erkenntlich gemacht habe.

Graz, im Jänner 2012

Acknowledgements

At first I want to express my gratitude to AO.Univ.-Prof. Dipl.-Ing. Dr.techn. M.Sc. tit. Univ.-Prof. Helmut Schweiger who made it possible for me to write this Master thesis. I am thankful for his efficient guidance and indicatory advices throughout my investigations.

I also want to thank Univ.-Ass. Dipl.-Ing. Franz Tschuchnigg for his cooperativeness, his valuable advices and his friendly supervision which made a quick and an efficient execution of my examinations possible.

Moreover, I am grateful that Dipl.-Ing. Dr.techn. Harald Krenn (STRABAG SE) supplied the subject for my thesis and all relevant information from the site to carry out my studies. I also want to thank him for his reliable and quick responding to any site-related issues and requests.

Finally I want to express special thanks to my parents. Without their prayers, their precious advices throughout the years of study, their patience and their willingness to financially support me I would not have been able to graduate at university.

Abstract

A tunnel facility project at Niagara Falls, Canada forms the background of this thesis. The aim of the tunnel project is to divert water from the Niagara River to an existing outtake structure. The typical cross section of the tunnel basically consists of a shotcrete lining, a membrane layer and a final lining. In order to pre-stress the final lining grout is injected between the membrane layer and the shotcrete.

The aim of this master thesis is to simulate the pre-stressing pressure on the final lining in PLAXIS 2010.

Assuming a constant pressure distribution along the tunnel perimeter the radial displacements and the normal force in the lining can be solved analytically and compared with the results of the Finite-Element calculation. Since the analytical solution is approximated with sufficient accuracy the numerical modelling of pre-stressing succeeds.

Furthermore, an unsymmetrical pressure distribution is simulated in the analysis and the diametrical displacements of the final lining are compared with the results obtained from the site.

To carry out the pre-stressing in the FE-calculation a thin gap is modelled between the final lining and the shotcrete. During the calculations it is found that the modelling of the gap stiffness plays a fundamental role for the pressure application on the lining. The gap stiffness has to be reduced to a low value to guarantee full pressure admission on the lining.

The established FE-model can be used to estimate the actively applied pressure behind the final lining on the site.

The calculations are performed for the Mohr-Coulomb and Hoek-Brown model. Changing the material model does not affect the deformations of the final lining. Changing the K_0 value has also a negligible effect.

Finally, a Seeber-diagram based on the FE-results is developed and compared with the results from the site. According to the results on site 90% of $\bar{p}_i$ is sustained by the rock material while the FE-analysis predicts 86%. Conclusively, the calculated partitioning of $\bar{p}_i$ matches with the obtained results on site.

Kurzfassung

Hintergrund der Arbeit bildet ein Tunnel Projekt bei den Niagara Fällen in Kanada. Ziel des Projektes ist es, Wasser aus dem Niagara River abzuleiten und einem bestehenden Auslaufbauwerk zuzuführen. Der Regelquerschnitt des Tunnels besteht aus einem Spritzbetonring, einer Abdichtungsfolie und der Ausbauschale. Um die Ausbauschale vorzuspannen, wird zwischen Spritzbeton und Abdichtungsfolie eine Zementinjektion eingepresst.

Ziel der vorliegenden Masterarbeit ist es, die Vorspannung der Ausbauschale in PLAXIS 2010 zu simulieren.

Die Verschiebungen sowie die Normalkraft in der Schale werden mit einer analytischen Lösung berechnet und mittels Finite-Element Berechnung hinreichend genau angenähert. Daraus folgt, dass das verwendete Modell die Vorspannung korrekt simuliert.

Des Weiteren wird eine unsymmetrische Druckverteilung hinter der Ausbauschale modelliert. Die radialen Verschiebungen der Schale werden mit den Ergebnissen vor Ort verglichen.

Um die Vorspannung im FE-Modell zu simulieren, wird ein schmaler Spalt zwischen der Ausbauschale und der Spritzbetonsicherung im Modell definiert. Die Steifigkeit des Spalts muss auf einen geringen Wert reduziert werden um den gesamten Vorspanndruck auf die Ausbauschale abzuleiten.

Das erstellte Rechenmodell kann zur Abschätzung der vor Ort auftretenden Vorspanndrücke verwendet werden.

Die Berechnungen werden mit den Mohr-Coulomb und Hoek-Brown Modell durchgeführt. Die Tunnelverformungen bleiben von der Änderung des Materialgesetzes unbeeinflusst. Dies trifft gleichermaßen auf die Variation von K_0 zu.

Abschließend wird anhand der FE-Ergebnisse ein Seeber-Diagramm erstellt und mit den Resultaten vor Ort verglichen. Der vom Fels aufgenommene Anteil des Innendrucks $\bar{p}_i$ wird vor Ort mit 90% angegeben, die FE-Berechnungen ergeben 86%. Daraus ist zu erkennen, dass die Aufteilung von $\bar{p}_i$ mit den Ergebnissen vor Ort übereinstimmt.

Table of contents

1 Introduction

1.1 Project description [1]

1.1.1 General

The aim of the Niagara Tunnel Facility Project is to divert water from the Niagara River to an existing storage reservoir. The tunnel extends to a length of approximately 10,4 km. The tunnel facility is planned to transport 500m³/s of water to the reservoir.

1.1.2 Longitudinal section

The longitudinal section of the tunnel project is included in Appendix (1). Besides, the stratigraphy, various geotechnical parameters and information on the applied grouting pressures along the tunnel chainage are included. It can be seen that the tunnel structure is mainly situated in the Queenston formation.

1.1.3 Typical cross section

The typical cross section consists of an initial shotcrete lining, a final concrete lining, a waterproofing membrane layer and a grouting system which is necessary to carry out the pre-stressing of the final lining and the surrounding rock. The internal diameter of the tunnel structure is 12,6 m. A drawing of the typical cross section can be found in Appendix (2).

1.1.4 Interface grouting

During the pre-stressing procedure grout is injected in the gap between the membrane layer and the shotcrete lining. Therefore, a system of grout-hose-rings is installed on the shotcrete which are used for the distribution of the grout. The ends of the hoses are guided through the membrane layer and the final lining into the tunnel interior. Due to the pre-stressing the final lining can sustain the internal water pressure and reinforcing the final lining is not required.

1.2 Statement of the problem

The aim of this thesis is on the one hand the correct numerical modelling of the interface grouting pressure. On the other hand, a distribution of the pre-stressing pressure along the tunnel lining which causes similar displacements as measured on site has to be found. The calculations are performed with the Mohr-Coulomb model and the Hoek- Brown material model. Finally, a Seeber-diagram based on the FE-results has to be developed in order to compare the results obtained on site.

2 Numerical modelling of interface grouting pressure

In order to verify the calculated forces and displacements of the final lining, an analytical solution is investigated and compared with the FE-results. Furthermore, the modelling of constant and unsymmetrical pressure admission along the tunnel perimeter is presented for the MC-model and the HB-model. Finally, a Seeber-diagram is set up based on the FE-results.

2.1 Analytical solution for a circular ring under external pressure

During the interface grouting procedure grout is injected between the waterproofing system and the initial lining. Consequently, the final lining and the surrounding rock are compressed. As illustrated in Figure 1 it is possible to divide the pre-stressing into two different load cases.

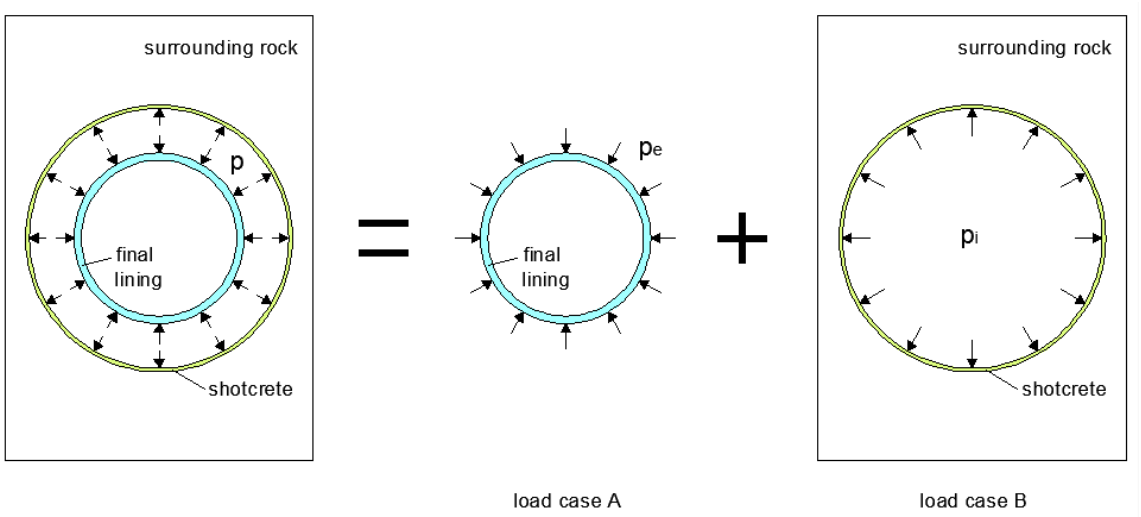

Fig. 1: Separation of pre-stressing into load case A and B.

With the following assumptions the equations for the stresses and deformations of the circular ring (load case A) and the surrounding rock material (load case B) can be solved analytically [2]:

- Elastic material behaviour of the lining
- Elastic, homogeneous and isotropic behaviour of the rock
- Constant pressure distribution around the lining

Furthermore, analytical solutions are available for load case B accounting for elasto-plastic or anisotropic behaviour of the rock.

In the following the analytical solution for load case A is discussed in further detail.

The circular ring in Figure 2 represents the tunnel final lining which is geometrically defined by an internal and external radius. The given material parameters E and ν indicate elastic behaviour of the final lining. As illustrated in Figure 2 the lining is loaded under a constant pressure distribution which causes stresses and deformations in the lining. Of interest are the tangential stresses σ_t in order to calculate the normal force, as well as the radial displacements Δr.

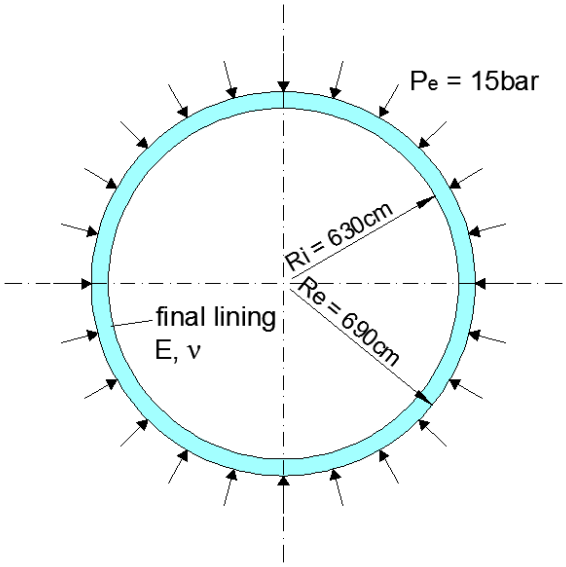

Fig. 2: Final lining under external pressure.

The tangential stresses σ_t and the radial displacements Δr are calculated according to the theory of the "thick- walled pipe" [3]. σ_t is determined as follows:

$$\sigma_t = \frac{1}{(r_e^2 - r_i^2)} * \left[p_e * r_e^2 * \left(1 + \frac{r_i^2}{r_x^2}\right) - p_i * r_i^2 * \left(1 + \frac{r_e^2}{r_x^2}\right) \right] \quad \textbf{Eq. 1}$$

where

σ_t … tangential stress [kN/m²]

r_e … external radius [m]

r_i … internal radius [m]

r_x … variable radius [m]

p_e … external pressure [kN/m²]

p_i … internal pressure [kN/m²]

As can be seen from Figure 2 the internal pressure on the final lining is zero ($p_i = 0$). Consequently, Eq. 1 reduces to:

$$\sigma_t = \frac{1}{(r_e^2 - r_i^2)} * \left[p_e * r_e^2 * \left(1 + \frac{r_i^2}{r_x^2}\right) \right] \quad \textbf{Eq. 2}$$

For plane strain conditions Δr_x is determined using the following formula [2]:

$$\Delta r_x = \frac{1}{E*(r_e^2 - r_i^2)} * \left[p_i * r_i^2 * \left(\frac{r_e^2}{r_x^2} * (1+\nu) + 1 - \nu - 2\nu^2\right) - p_e * r_e^2 * \left(\frac{{r_i}^2}{{r_x}^2} * (1+\nu) + 1 - \nu - 2\nu^2\right)\right] \quad \textbf{Eq. 3}$$

where

Δr_x … radial displacement [mm] (for arbitrary radii within the lining)

r_e … external radius [m]

r_i … internal radius [m]

r_x … variable radius [m]

p_e … external pressure [kN/m²]

p_i … internal pressure [kN/m²]

E … E- modulus [kN/m²]

ν … Poisson's ratio [-]

Since the internal pressure is zero Eq. 3 reduces to:

$$\Delta r_x = \frac{p_e * r_x * {r_e}^2}{E*(r_e^2 - r_i^2)} * \left[\frac{{r_i}^2}{{r_x}^2} * (1+\nu) + 1 - \nu - 2\nu^2\right] \quad \textbf{Eq. 4}$$

2.1.1 Resulting normal force

The tangential stresses are calculated as defined in Eq 2. With the given radii of the final lining and p_e = 1500 kN/m² σ_t results in

r_e = 6,90 m

r_i = 6,30 m

r_m = 6,60 m

$$\sigma_t = \frac{1}{(6{,}90^2 - 6{,}30^2)} * \left[1500 * 6{,}90^2 * \left(1 + \frac{6{,}30^2}{6{,}60^2}\right)\right] = 17\,232{,}99\ kN/m^2$$

Taking the thickness of the final lining into account (t = 0,60m), the resulting normal force is

$$N = \sigma_t * A = 17\,232{,}99\ \frac{kN}{m^2} * 0{,}6\ m * 1{,}0\ m = 10339{,}79\ kN/m$$

2.1.2 Radial displacements

Eq. 4 defines the calculation of the radial displacements. Using the given material parameters E and ν of the concrete Δr in the middle of the lining is calculated as follows:

with

E = 26 600 MN/m²

ν = 0,2

$$\Delta r_m = \frac{1500 * 6{,}60 * 6{,}90^2}{26\,600 * (6{,}90^2 - 6{,}30^2)} * \left[\frac{6{,}30^2}{6{,}60^2} * (1 + 0{,}2) + 1 - 0{,}2 - 2 * 0{,}2^2\right] = 4{,}06\ mm$$

2.2 Available tools in PLAXIS for the modelling of grout pressure

In general, the most suitable way to model grout pressure in PLAXIS is to apply a pore pressure on a soil cluster. PLAXIS allows two different options as shown in Figure 3 and Figure 4:

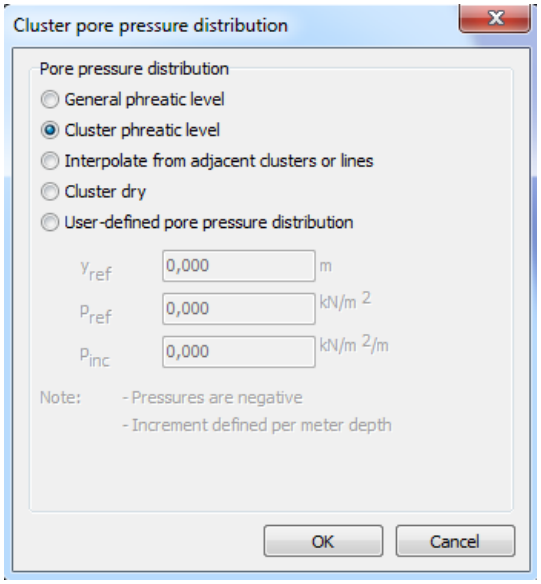

Fig. 3: Cluster phreatic level option.

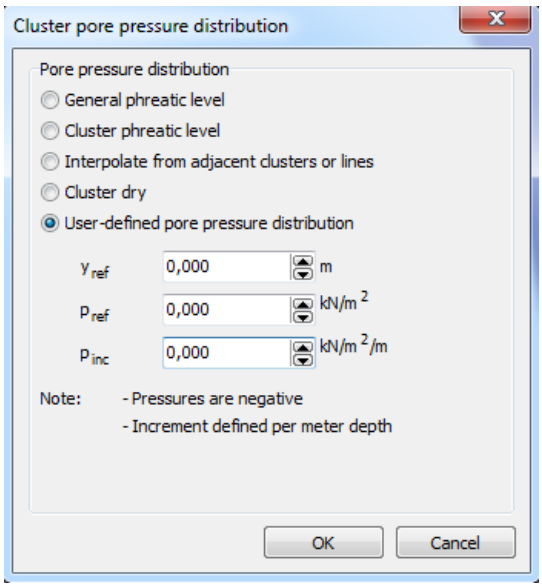

Fig. 4: User-defined pore pressure distribution.

In order to find out which of the two presented options is more appropriate in case of pore pressure application along a tunnel a simplified model is set up.

Figure 5 shows the geometry of the simplified model. It consists of non- porous layers at the bottom and the top and a soil layer in between. The arrangement of the three layers in the simplified model is comparable to the lining composition of the tunnel which basically consists of two non- porous layers (shotcrete and final lining) and a gap in between. The gap opens up when the grouting procedure starts and is immediately filled with non-hardened grout material. The weak grout material at the beginning of the procedure is represented by the soil layer in the simplified model.

The material parameters for the model are given in Table 1.

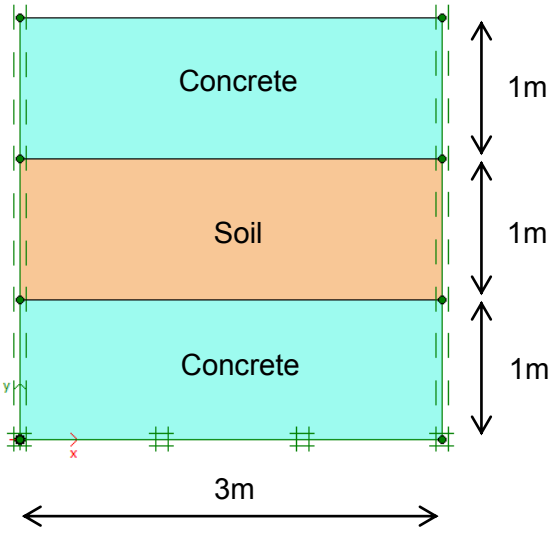

Fig. 5: Geometry of the simplified model.

	Concrete	Soil
E- modulus [MPa]	25 000	100
ν [-]	0,2	0,2
γ_{unsat} [kN/m³]	24	19

Tab. 1: Linear elastic material parameters used in the simplified model.

The calculations are performed in two different ways. In the first calculation the “user defined pore pressure distribution” is selected to generate pore pressures in the soil layer. Afterwards the “cluster phreatic level” tool is applied. Both calculations consist of the following calculation phases:

- Initial phase (no groundwater)
- Pressure phase

In the first calculation a pore pressure of 1 bar is applied on the soil cluster. Figure 6 illustrates the pore pressure distribution in the soil cluster after the pressure phase.

In the second calculation the “cluster phreatic level” option is applied. In order to generate a pore pressure of 1 bar at the bottom edge of the soil layer the water table of the soil cluster has to be defined at y = 2,0m. In Figure 7 the pore pressure distribution in the soil cluster can be seen.

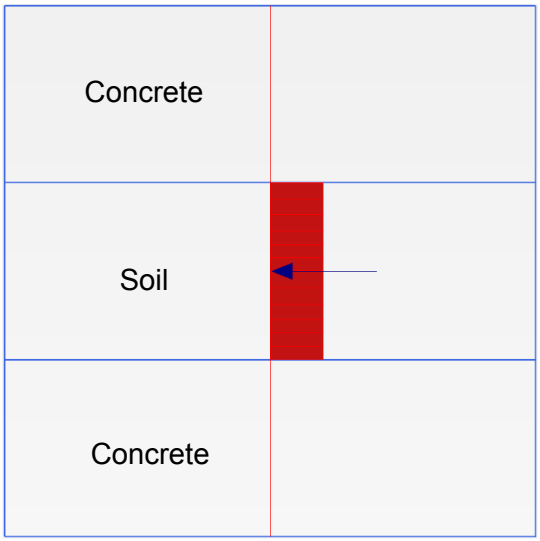

Fig. 6: Pressure distribution for „User- defined pressure distribution“. Max. = Min. = -10 kN/m².

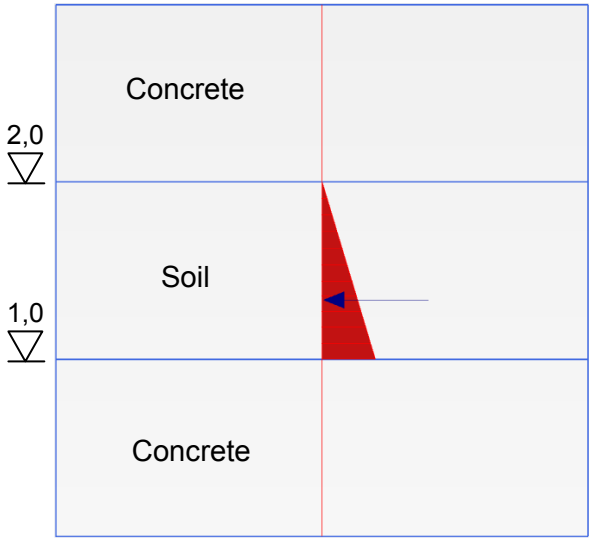

Fig. 7: Pressure distribution for „Cluster phreatic level“. Max. = 0 kN/m². Min. = -10 kN/m².

From Figure 6 it can be seen that the pore pressure distribution is constant over the soil layer when using the “user- defined pore pressure distribution”. For the second calculation the pore pressure increases linearly with the soil depth as demonstrated in Figure 7.

The increase of the pore pressure in Figure 7 results from the unit weight of the water which also applies for the injection grout on site. Due to the high operating pressures on site the influence of the unit weight is neglected and the distribution of the injection grout over the height of the gap is assumed to be constant.

The application of the “cluster phreatic level” option is acceptable as long as the cluster is straight lined and orientated horizontally or vertically. Since this is not the case for the gap clusters along the tunnel lining the application of “cluster phreatic level” is tricky.

Therefore, it can be concluded that for further calculations in PLAXIS the “user- defined pore pressure distribution” is the appropriate option to simulate the injection pressure along the tunnel lining.

2.3 Constant pressure admission on the tunnel lining

In order to perform the calculations presented in this chapter it is necessary to select relevant cross sections along the tunnel alignment. This decision is based on the longitudinal section of the tunnel project which is included in Appendix (1).

2.3.1 Calculation Section 1

Calculation Section 1 is located at chainage km 1 + 411.000 which is close to the deepest point of the tunnel. As illustrated in the longitudinal section Calculation Section 1 is situated within the area of highest grouting pressures. Additionally, detailed information on the rock layer formation is available for this chainage.

2.3.1.1 Geometry and materials

In the Appendix (3) the cross section at km 1 + 411.000 is illustrated. The tunnel is exclusively located in the Queenston Q9- Q6 formation. The groundwater table is situated about 36m below the ground surface. Since the Rochester formation acts as an aquitard the inflow of groundwater is predicted to be low. Furthermore, any water inflow is covered by standard pumping measures on site [1]. Consequently, the groundwater is not taken into account for further calculations.

With a specific weight of γ_R = 26 kN/m³ for all rock formations and an assumed γ_O = 15 kN/m³ for the overburden the vertical initial stresses at the top edge of the Queenston Q9- Q6 layer are calculated as follows:

$$\sigma'_{yy} = 15{,}0\,\frac{kN}{m^3} * 16{,}0m + 26{,}0\,\frac{kN}{m^3} * 77{,}0m = 2242\ kN/m^2$$

To reduce the height of the FE-model all rock layers above the Queenston Q9- Q6 formation are substituted by a dummy layer. This simplification is admissible since the displacements in the upper rock layers are not of importance. The height of the dummy layer is assumed to be 3,0m. In order to generate the same vertical initial stresses σ'_{yy} as demonstrated above the required specific weight of the dummy layer is equal to:

$$\gamma_{dummy} = \frac{2242\ kN/m^2}{3{,}0m} = 747{,}\dot{3}\ kN/m^3$$

Figure 8 demonstrates the geometry model for the FE-analysis. The dimensions of the model are determined according to the following empirical formulas:

$$distance\ to\ bottom = 2 * d = 2 * 12{,}6m = 25{,}2m \rightarrow chosen\ 25m$$

$$width = 2 * (4 * d) = 2 * (2 * 12{,}6m) = 100{,}8m \rightarrow chosen\ 120m$$

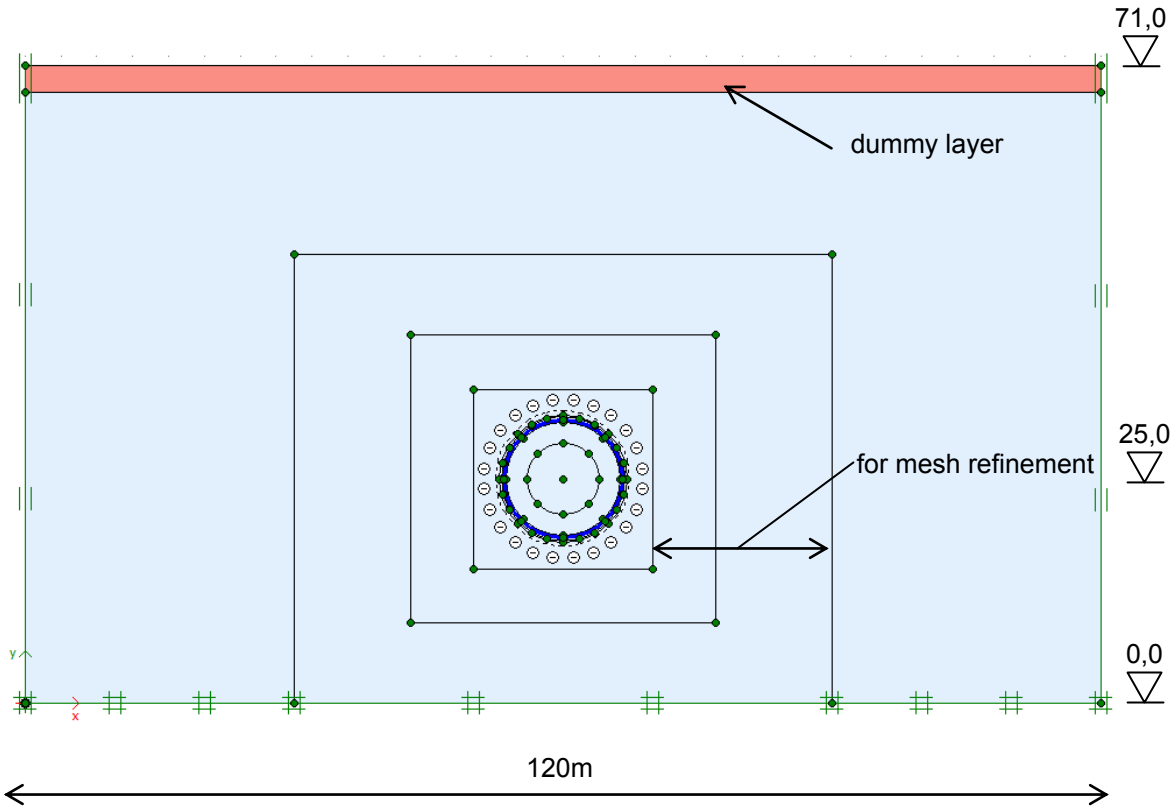

Fig. 8: Geometry model for Calculation Section 1.

The cross section of the tunnel and a detail of the different tunnel linings are presented in Figure 9.

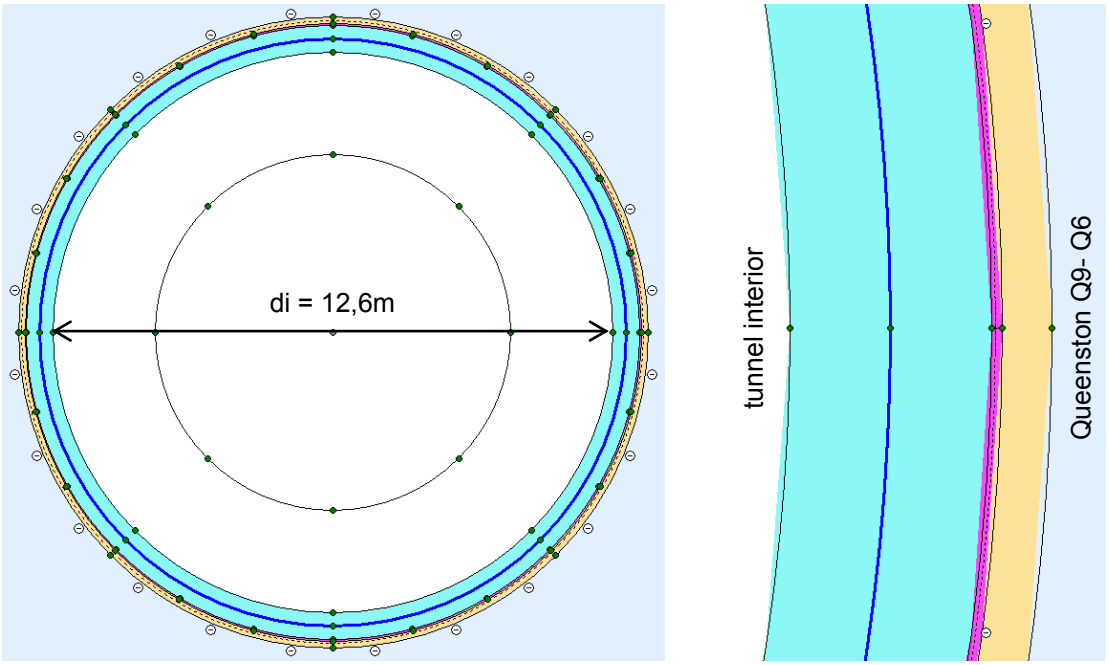

Fig. 9: Tunnel and lining detail. Thickness of final lining = 60cm, gap = 3cm and shotcrete = 15cm.

For the set up of the tunnel cross section the “tunnel designer” is used. The final lining and the shotcrete as well as the gap material are modeled as continuum elements. As illustrated in Figure 9 a plate element is included in the middle of the final lining in order to evaluate the resulting normal force. The flexural rigidity EI as well as the axial stiffness EA are reduced to a negligible magnitude in order to avoid influences on the internal forces of the lining. Figure 10 shows the defined plate parameters.

Fig. 10: Material properties of the plate element in the final lining.

As shown in Figure 9 an interface is attached on the outside of the final lining. The interface is used later on whether to check if the full pore pressure is applied on the final lining. Further details on the implementation of the interface can be found in Chapter 2.3.1.6.

The rock materials as well as the different lining materials are defined as “soil and interface”. In order to describe the material behaviour of the rock the Mohr-Coulomb model is applied. The tunnel linings and the gap material are defined linear elastic. The required input parameters are given in Table 2 and 3.

Mohr-Coulomb	γ_{unsat} [kN/m³]	γ_{sat} [kN/m³]	E [kN/m²]	ν [-]	c [kPa]	φ [°]	ψ [°]	K_0 [-]
Queenston Q9-Q6	26	26	13,60E06	0,2	1100	41,4	0	1,5
Dummy layer	747,3	747,3	13,60E06	0,2	1100	41,4	0	1,5

Tab. 2: Material properties for the Mohr-Coulomb model.

Linear elastic	γ_{unsat} [kN/m³]	E [kN/m²]	ν [-]
Final lining	24	26,60E06	0,2
Shotcrete	24	15,00E06	0,2
Gap material	19	15,00E06	0,2
Soft gap material	19	50	0,2

Tab. 3: Material properties using the linear elastic model.

After the completion of the material input the FE-mesh has to be generated. To keep the number of elements to a minimum a global coarseness of “very coarse” is selected. Around the closer vicinity of the tunnel a mesh refinement is carried out as demonstrated in Figure 11. Due to the small thickness of the gap the element size factor for geometry lines and points has to be reduced in order to allow for successful mesh generation. This applies in particular for the gap clusters as well as for the lining clusters. The local element size factor for all geometry lines of the tunnel lining is defined as 0,1. For the geometry points of the linings the element size factor amounts to 0,05. In total a number of 2728 elements is produced.

Figure 11 represents the generated mesh for the whole model. A mesh detail of the linings and the gap can be seen in Figure 12.

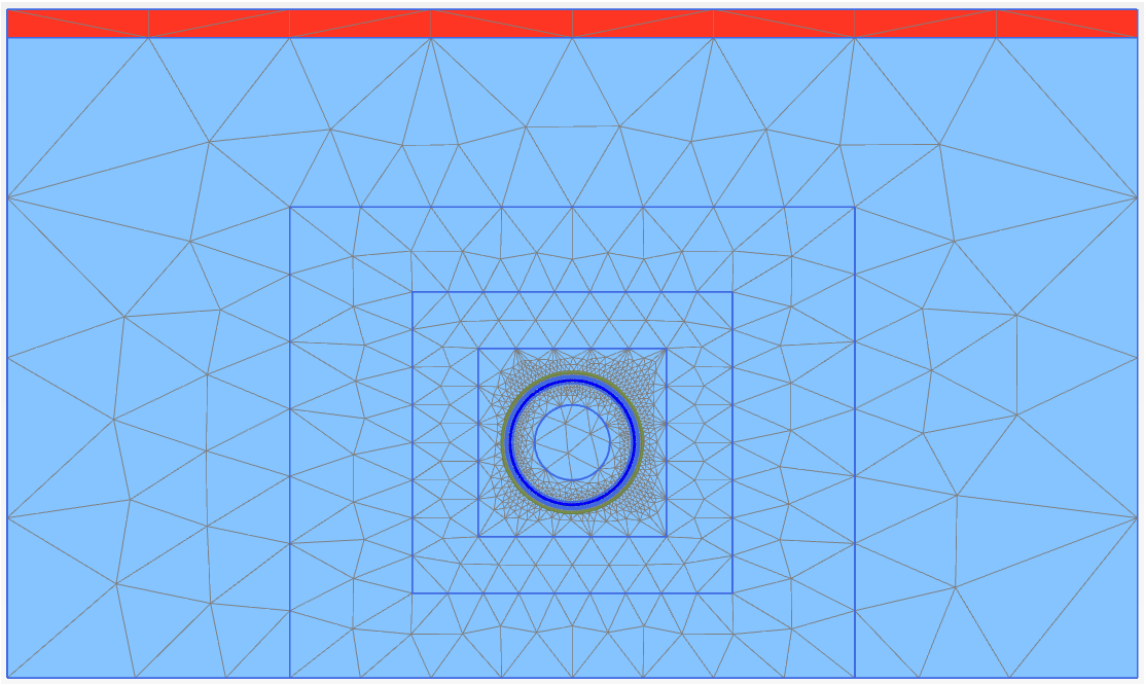

Fig. 11: Generated mesh illustrated for the whole model.

.

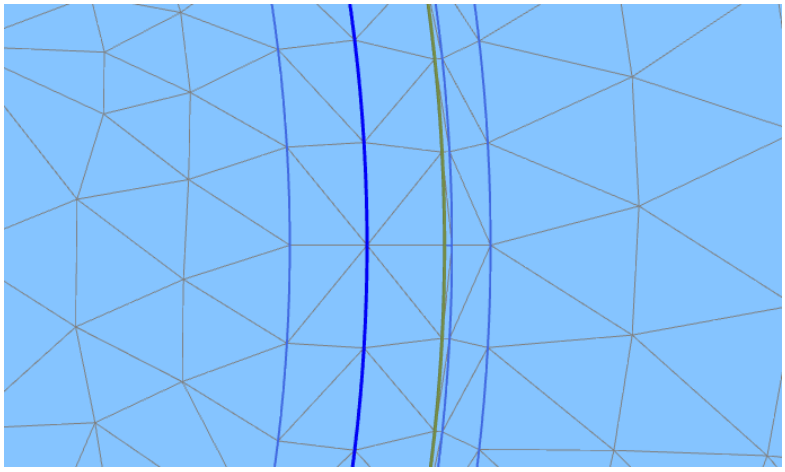

Fig. 12: Detail view of the generated mesh in the closer area of the tunnel linings.

2.3.1.2 Calculation phases

The calculations are performed in five different phases as shown in Figures 13- 17.

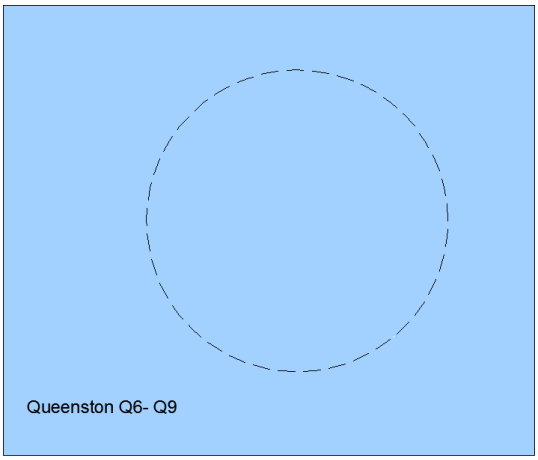

Fig. 13: 0. Initial phase (K_0 = 1,5).

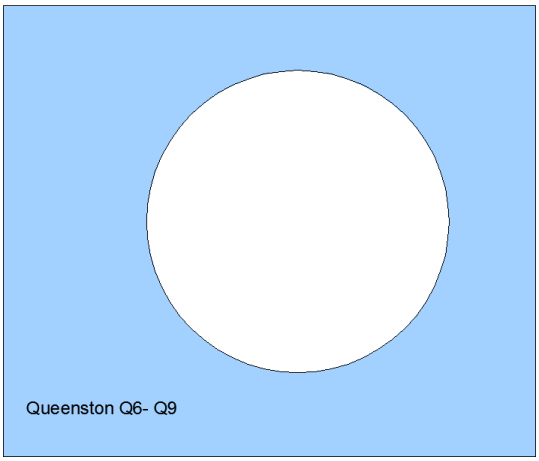

Fig. 14: 1. Excavation (M_{stage} = 0,2).

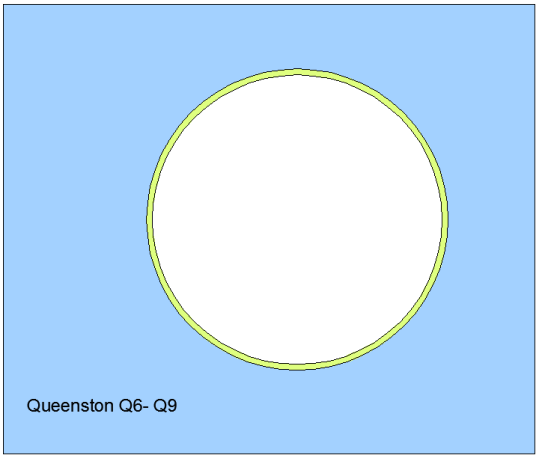

Fig. 15: 2. Activation shotcrete (M_{stage} = 1,0).

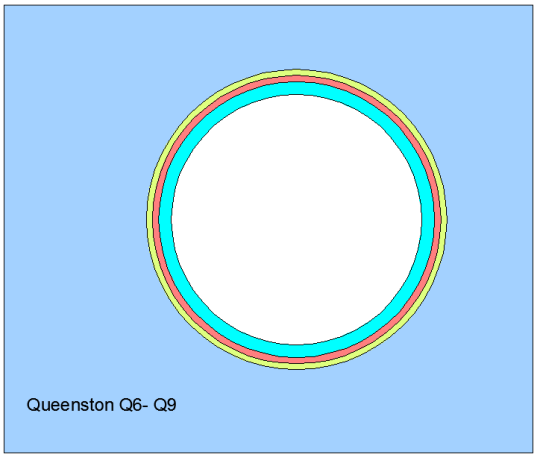

Fig. 16: 3. Activation gap material & final lining.

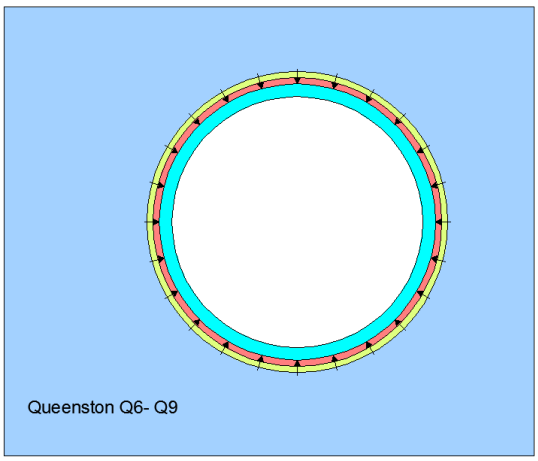

Fig. 17: 4. Pressure phase (p = 15 bars, E_{gap} <<).

The calculation type for the initial phase is performed as "K_0 procedure". A K_0 value of 1,5 is chosen for this study.

Phase 1- 4 are performed as "plastic" analysis. In the excavation phase M_{stage} is limited to 0,2 in order to account for pre-relaxation effects. When activating the shotcrete lining in phase 2 M_{stage} is set to 1,0.

In phase 3 the final lining and the gap material are activated. The stiffness of the gap material is the same as the shotcrete stiffness. In the last phase a constant pressure distribution of 15 bars is applied around the tunnel lining. Important for phase 4 is, that the stiffness of the gap has to be reduced to a low value (E = 50 kPa) in order to guarantee full pressure application on the lining. Further details on the correlation between the gap stiffness, the resulting normal force and the lining displacements are included in Chapter 2.3.1.4.

2.3.1.3 Results

Of interest are the deformations of the final lining as well as the resulting normal force after applying the pore pressure. In a first approach the results for Calculation Section 1 are compared with the results for the analytical solution as demonstrated earlier in chapters 2.1.1 and 2.1.2.

Figure 18 represents the horizontal and vertical phase displacements of the lining. The resulting normal force is illustrated in Figure 20.

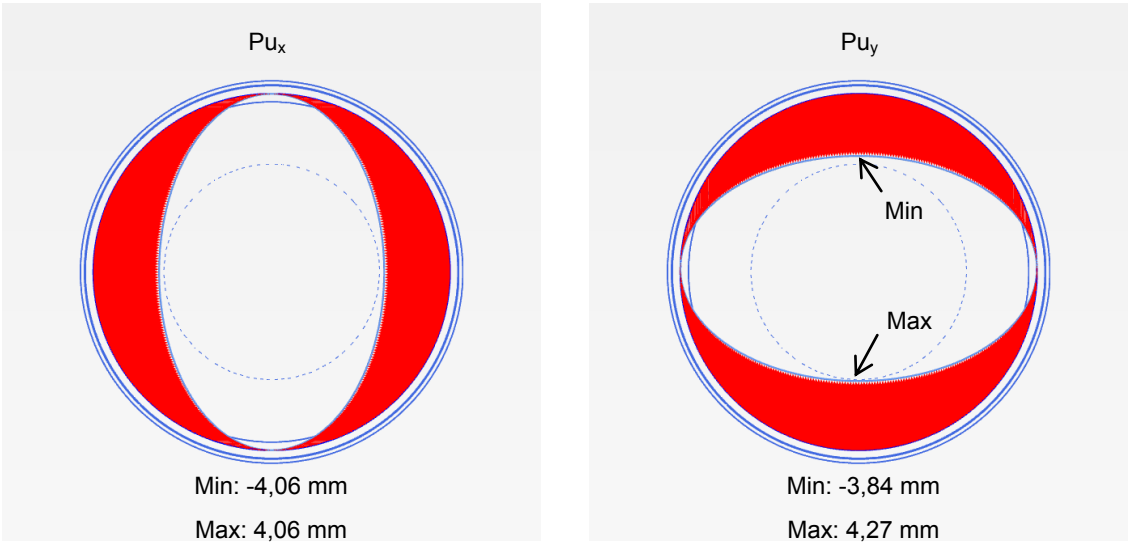

Fig. 18: Pu_x and Pu_y of the final lining after applying the pore pressure.

From Figure 18 it can be seen that Pu_y is not distributed symmetrically along the horizontal tunnel axis what indicates an influence of the bottom boundary on the vertical displacements. As a result the entire tunnel structure is lifted during the pore pressure application.

Figure 19 demonstrates the displacements in the surrounding rock after the application of the pore pressure. It can be seen that the largest displacements in the rock occur above the tunnel.

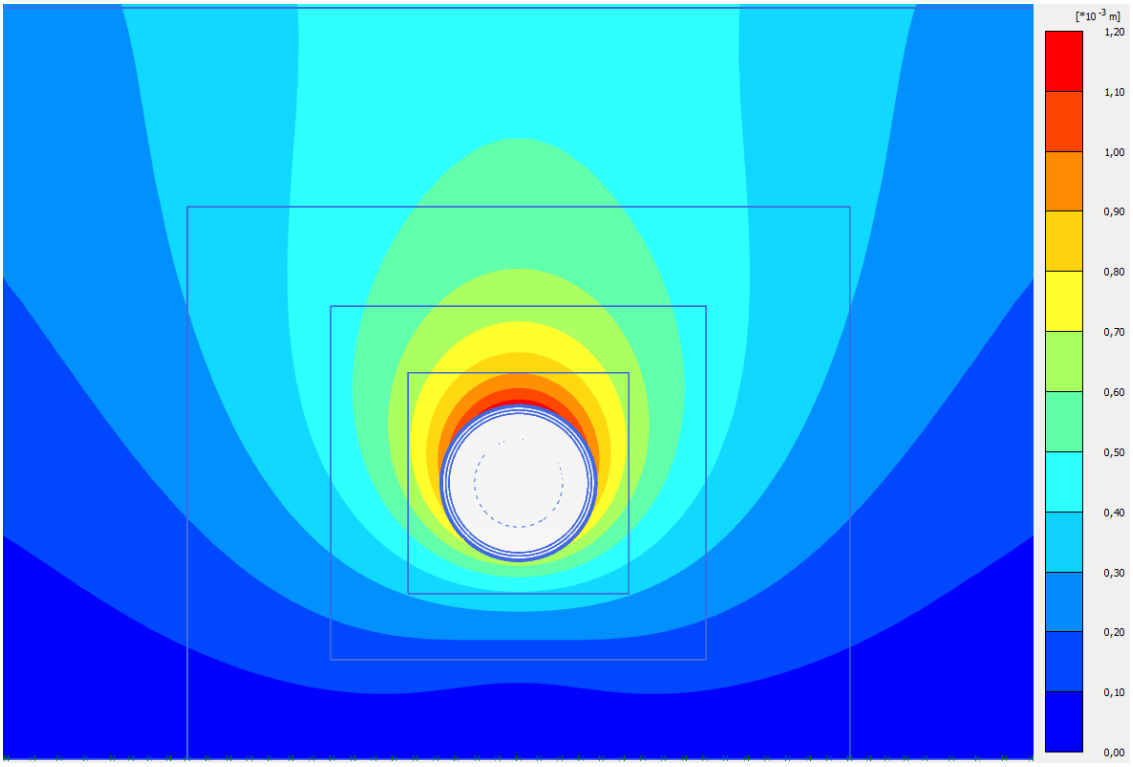

Fig. 19: Phase displacements |Pu| after the pore pressure application.

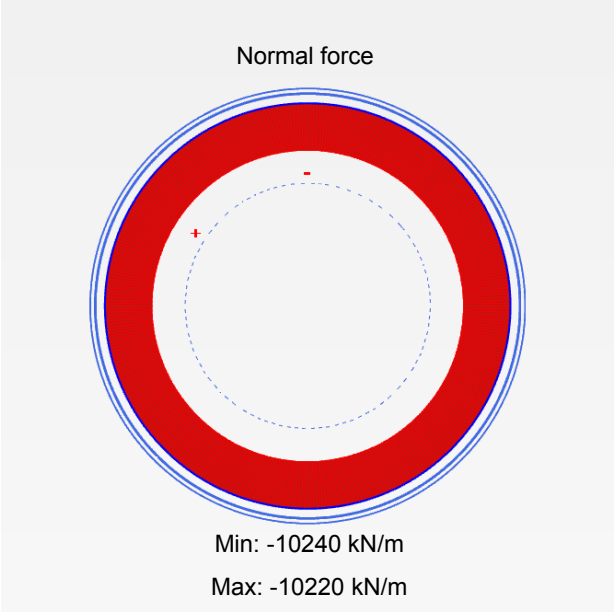

Fig. 20: Results for N_{max} and N_{min} scaled up by the factor 10^4.

Finally, the FE-results are compared with the results of the analytical solution. The divergence Δ between the two different solutions is presented in Table 4. In order to compare the normal forces a mean value of N_{max} and N_{min} is calculated.

	Analytical solution	FE-results	Δ
Normal force N	10334 kN/m	10230 kN/m	1%
Displacements Δr_m, Pu_x	Δr_m = 4,06 mm	Pu_x = 4,06 mm	0%

Tab. 4: Divergence Δ between the analytical solution and the FE-results.

From Table 4 it can be concluded that the implemented FE-model approximates the analytical solution with sufficient accuracy. Furthermore, the results emphasise that simulating the pre-stressing of a tunnel lining is generally possible for a constant pressure application along the tunnel perimeter.

2.3.1.4 Influence of E_{gap} on the lining displacements and the normal force

The correct modelling of E_{gap} during the pressure application has a significant influence on the resulting normal force and the deformation of the lining. This can be proved by varying the stiffness of the gap material. Therefore, a calculation is performed where the gap material in the pressure phase is defined with an increased E_{gap} of 15 GPa instead of 50 kPa. Figure 21 presents the normal force and the phase displacements Pu_x and it follows, as expected, that the results are not correct.

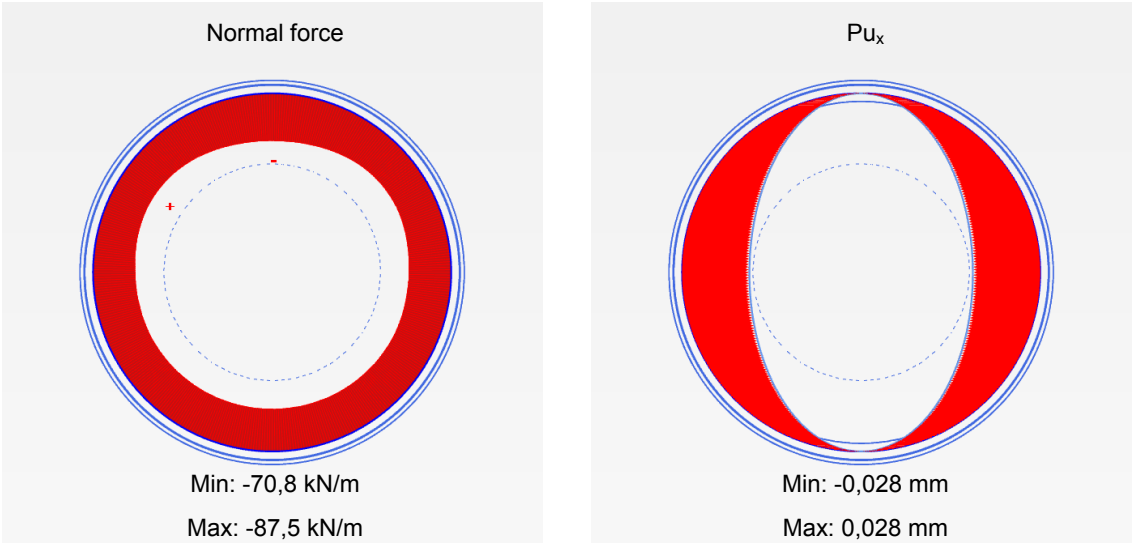

Fig. 21: N and Pu_x after the pressure application with E_{gap} = 15GPa.

2.3.1.5 Model variations for Calculation Section 1

In the following different modifications of the model specified in Chapter 2.3.1.1 are presented.

Due to effects of the bottom boundary Pu_x at the wall and Pu_y at the invert and the top are of different magnitudes (Figure 18). The stiffness of the rock material is increased from 13,6 GPa to 40 GPa in the first calculation and increased further to 90 GPa in the second step. Table 5 demonstrates the phase displacements after the pressure application for both cases.

	Pu_x	Pu_y
E_{rock} = 40 GPa	Max: 4,06 mm	Max: 4,11 mm
	Min: -4,06 mm	Min: -4,00 mm
E_{rock} = 90 GPa	Max: 4,06 mm	Max: 4,07 mm
	Min: -4,06 mm	Min: -4,04 mm

Tab. 5: Comparison of phase displacements for different E_{rock}.

The results in Table 5 indicate that the difference in Pu_x and Pu_y reduces as E_{rock} is increased. Additionally, Pu_y approaches Pu_x proving that Pu_x is more comparable to Δr_m from the analytical solution than Pu_y.

In a second approach the original stiffness of the rock is reduced. It is observed that the vertical translation of the entire tunnel structure grows as E_{rock} declines. This can be explained by the increasing influence of the bottom boundary on the vertical displacements when the rock stiffness is reduced.

Besides the tunnel deformations the variation of E_{rock} additionally affects the distribution of the normal force in the lining. As illustrated in Figure 20 a maximum and minimum value of N occur and therefore, the normal force is not distributed uniformly along the tunnel lining. The unequal distribution results from the vertical translation of the tunnel structure as well as from the self-weight of the final lining.

With the results in Table 6 it can be demonstrated that an increase of E_{rock} decreases the difference in max N and min N. Furthermore, the deactivation of the final lining weight leads to an equal distribution of the normal force.

	Original material parameters	Variation A
Normal force	Max: -10220 kN/m	Max: -10220 kN/m
	Min: -10240 kN/m	Min: -10220 kN/m

Tab. 6: N for the original parameters and Variation A where E_{rock} = 100 GPa and $\gamma_{final\ lining}$ = 1 kN/m³.

2.3.1.6 Comments on the interface in the tunnel cross section

As mentioned in Chapter 2.3.1.1 an interface is inserted between the final lining and the gap material. The general idea of the interface at this position is to find out if the pore pressure is fully applied on the final lining. This is carried out by evaluating the interface stresses before and after the pore pressure application.

A plot of σ_{tot} on the interface after the pressure application is illustrated in Figure 22. It can be seen that the pore pressure is fully applied on the tunnel lining.

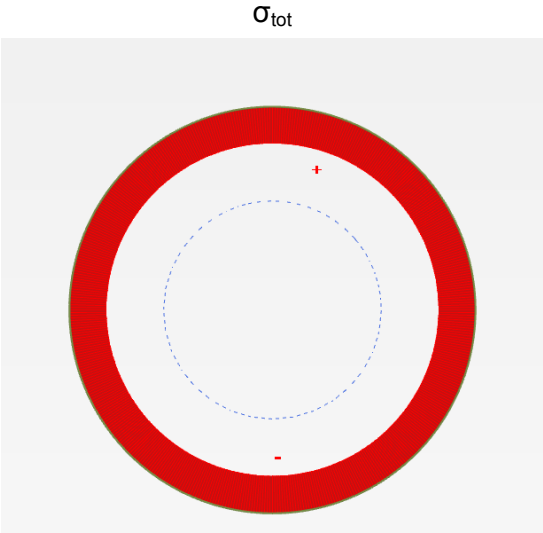

Fig. 22: σ_{tot} after applying the pore pressure.

Furthermore, calculations are performed using a second interface between the gap and the shotcrete lining as illustrated in Figure 23. At this point it has to be mentioned that the second interface has to be inserted inside the gap in order to guarantee a correct evaluation of the interface stresses. If the interface is placed in the shotcrete lining, the interface stresses in the shotcrete are calculated. In this case σ_{tot} is equal to σ' since per definition the pore pressure has be zero in a non-porous material.

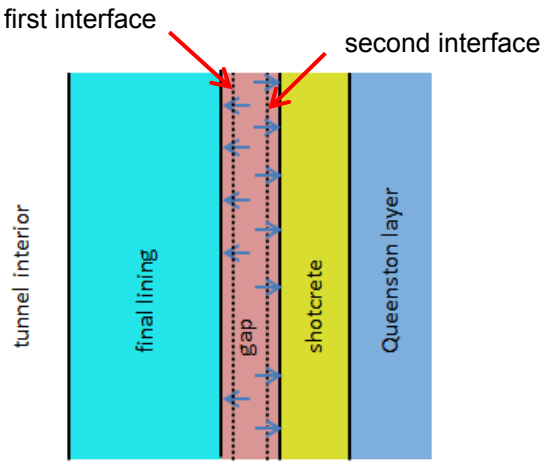

Fig. 23: Arrangement of interfaces in the gap material.

From the resulting stresses of the first and second interface it can be concluded that the pore pressure is fully applied on the final lining as well as on the shotcrete.

As mentioned in Chapter 2.3.1.4 the stiffness of the gap material affects the normal force in the lining and the deformations. In the following the influence of E_{gap} on the interface stresses is demonstrated.

Therefore, the gap stiffness is varied for Calculation Section 1. In the first calculation E_{gap} is increased from 50 to 2000 kPa. Secondly, the gap stiffness is enlarged to 200 MPa. The resulting interface stresses σ' and σ_{tot} are to be found in Figures 24 and 25.

E_{gap} = 2000 kPa

σ'

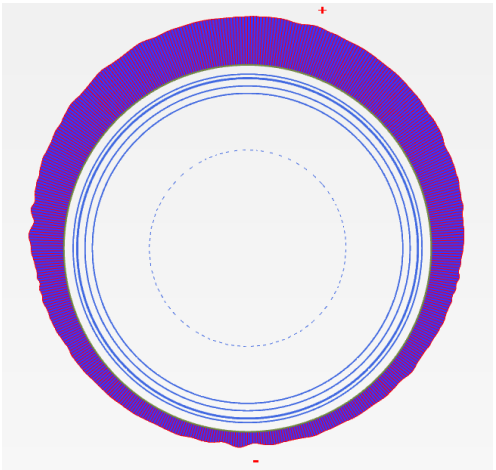

Min: 9,50 kN/m²
Max: 39,89 kN/m²

σ_{tot}

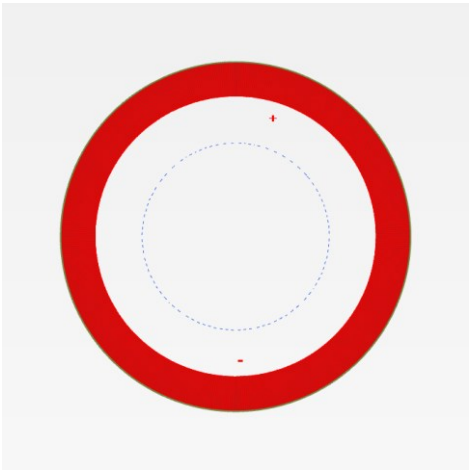

Min: -1491 kN/m²
Max: -1460 kN/m²

Fig. 24: Interface stresses for E_{gap} = 2000 kPa. σ_{tot} - σ' = u = 1500 kPa.

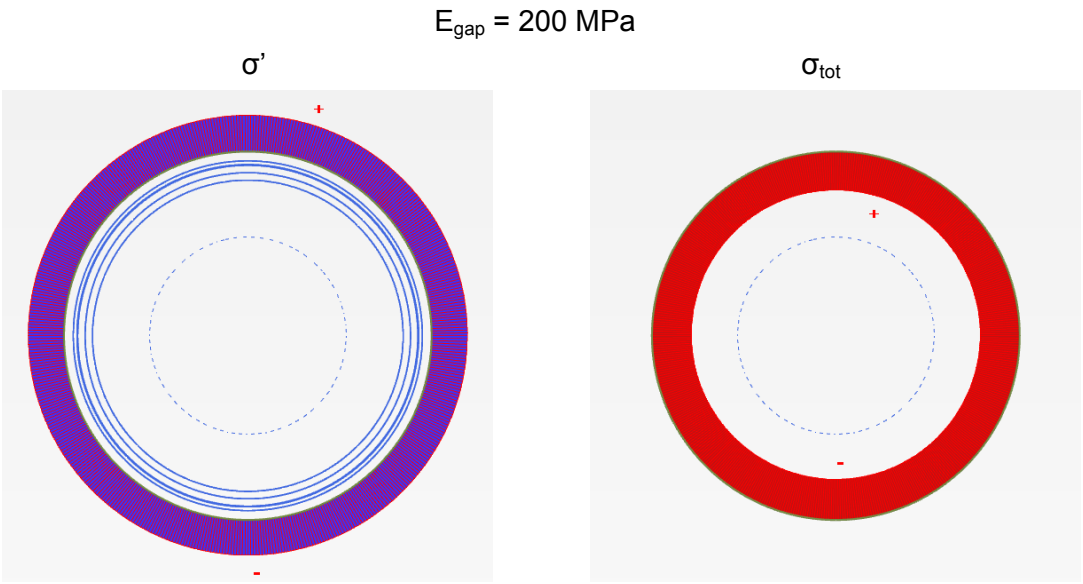

Fig. 25: Interface stresses for E_{gap} = 200 MPa. σ_{tot} - σ' = u = 1500 kPa.

The results in Figures 24 and 25 show that the interface stresses change if the gap stiffness is modified. The tensile stress σ' in the gap grows as E_{gap} is increased and therefore, the actively applied pressure σ_{tot} on the final lining reduces. As a result, the normal force in the lining is reduced as pointed out in Chapter 2.3.1.4.

2.3.2 Calculation Section 2

Monitoring results from the site are available for a chainage lower than the one from Calculation Section 1. In order to compare the calculated tunnel deformations of the FE-analysis with the results on site a second calculation section is set up and located at chainage km 0 + 726.939. The different rock layers at this chainage are defined as given in the longitudinal section (Appendix (1)).

2.3.2.1 Geometry and materials

The defined model for Calculation Section 2 is illustrated in Figure 26. As mentioned in Chapter 2.3.1.1 the groundwater table is not taken into account. At Calculation Section 2 the rock formations Power Glen, Whirlpool, Queenston Q10 as well as Queenston Q9-Q6 significantly affect the deformations of the tunnel lining. The Mohr-Coulomb parameters for the mentioned rock layers are included in Table 7.

	c [MPa]	φ [°]	E [GPa]
Power Glen	4,0	58	28,2
Whirlpool	6,1	59,4	82,0
Queenston Q10	0,8	39,0	7,7
Queenston Q9-Q6	1,1	41,4	13,6

Tab. 7: Mohr-Coulomb parameters for dominating rock formations at Calculation Section 2.

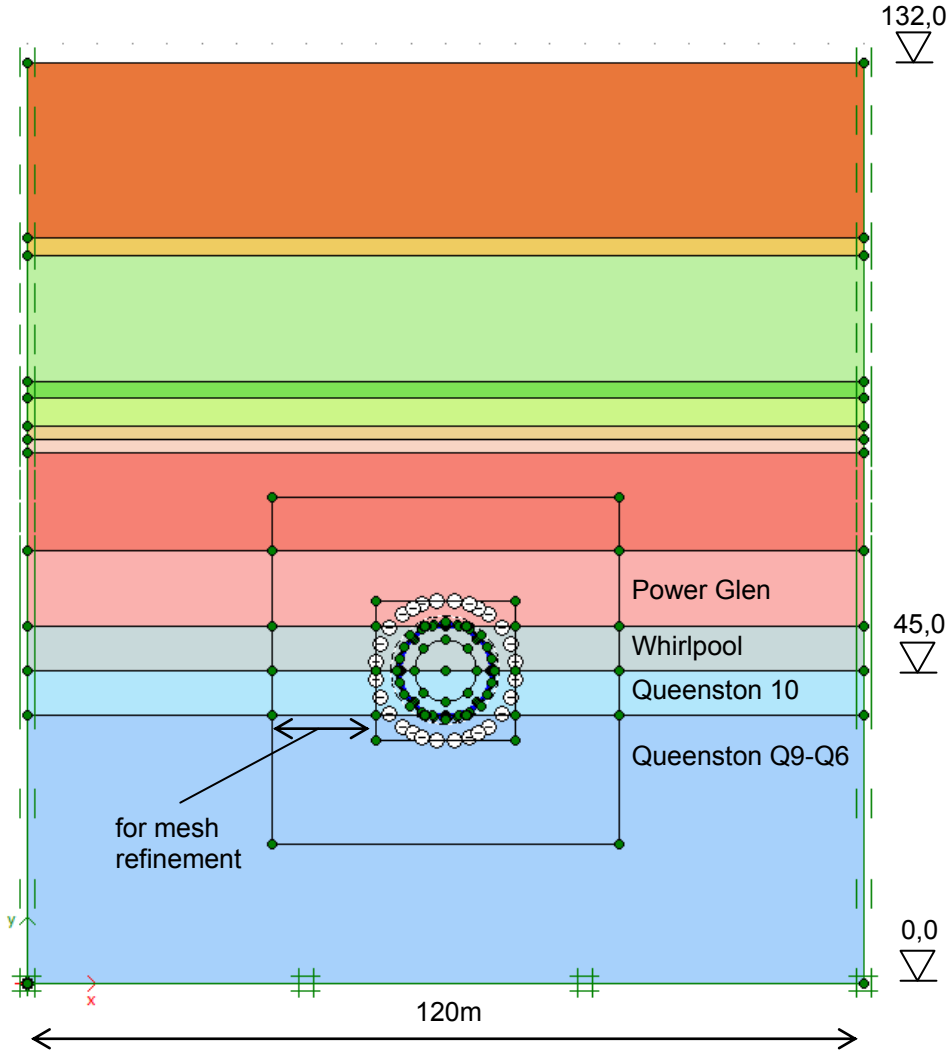

Fig. 26: Geometry model for Calculation Section 2.

The setup of the tunnel cross section, the material input and the generation of the mesh is carried out in analogy to Chapter 2.3.1.1. In total a number of 2332 elements are produced at Calculation Section 2.

The calculation is carried out as mentioned in Chapter 2.3.1.1.

2.3.2.2 Results

In order to illustrate the influence of the different rock layers on the tunnel deformations the deformed mesh for Calculation Section 1 and Calculation Section 2 is presented in Figure 27.

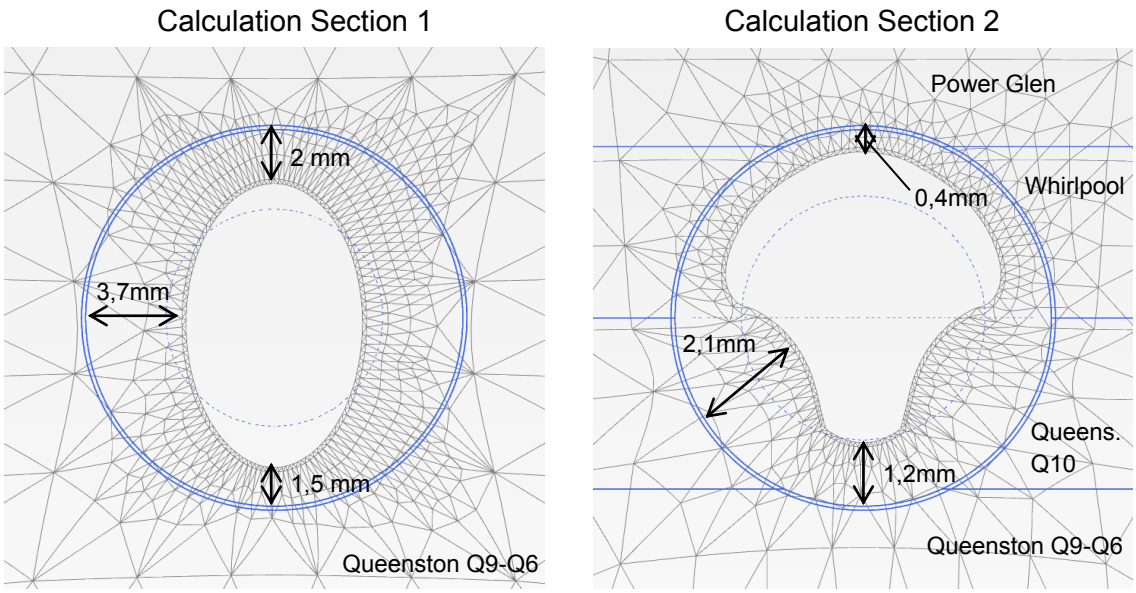

Fig. 27: Comparison of the total displacements |u| of Calculation Section 1 with Calculation Section 2 after activating the shotcrete.

The phase displacements Pu_x and Pu_y of the final lining after the pore pressure application are illustrated in Figure 28.

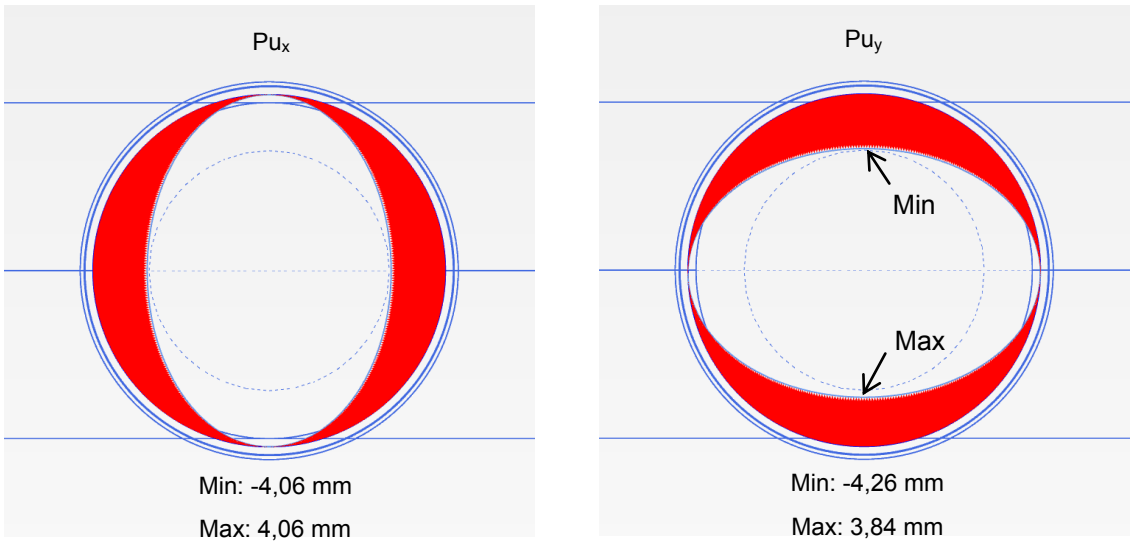

Fig. 28: Pu_x and Pu_y of the final lining after the pore pressure application.

The results in Figure 28 demonstrate that Pu_x are distributed symmetrically along the vertical tunnel axis. The magnitudes as well as the distribution of Pu_x are the same for Calculation Section 1 and 2.

From the distribution of Pu_y in Figure 28 it can be seen that the maximum vertical displacement occurs in the top of the tunnel. This can be explained by the fact that the stiffness of the upper rock layers (Whirlpool and Power Glen) is significantly higher compared to the stiffness of the lower rock formations. Consequently, the entire tunnel structure is slightly pushed into the softer Queenston material when applying the pore pressure.

Furthermore, the phase displacements |Pu| for the surrounding rock material after the pressure application are illustrated in Figure 29.

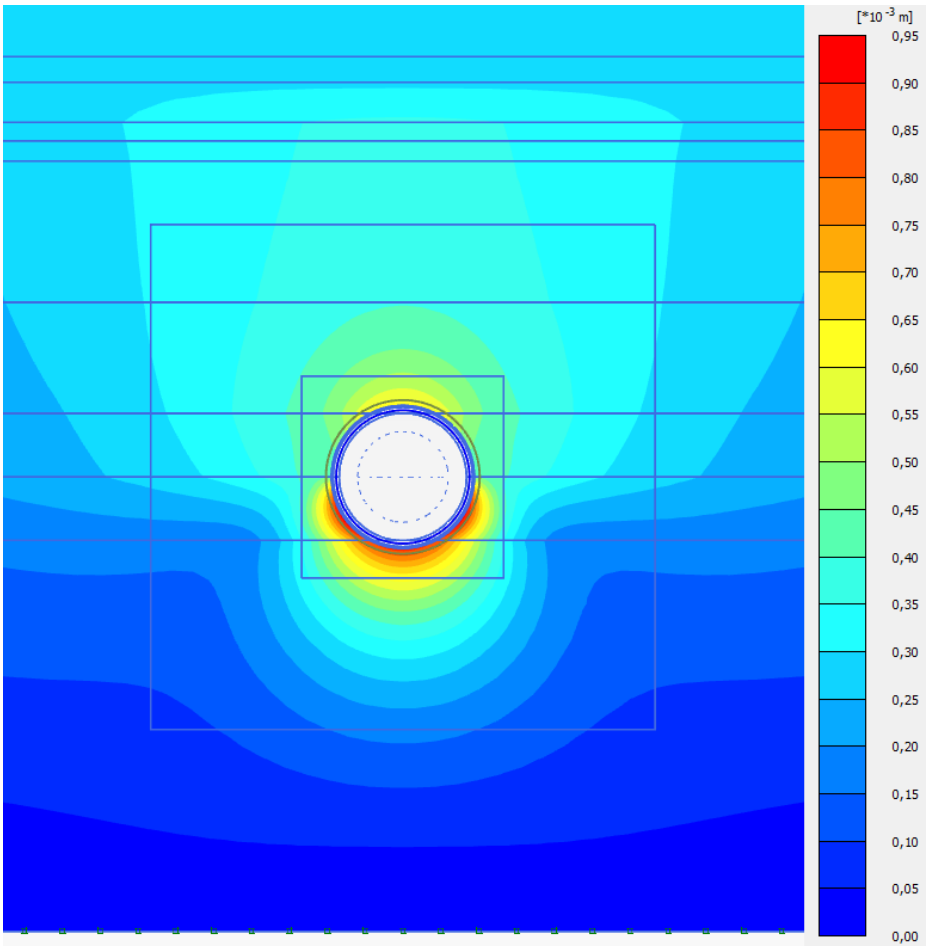

Fig. 29: Phase displacements |Pu| in the rock material after applying the pore pressure.

Compared to Calculation Section 1 the distance of the tunnel center to the bottom boundary in Calculation Section 2 is 20m higher. Therefore, the influence of the bottom boundary on the phase displacements of the rock material is reduced. As demonstrated in Figure 29 a uniform distribution of the pressure bulb appears in the Queenston material.

The resulting normal force is given in Figure 30. Additionally, the normal force and the displacements for both Calculation sections are given in Table 8.

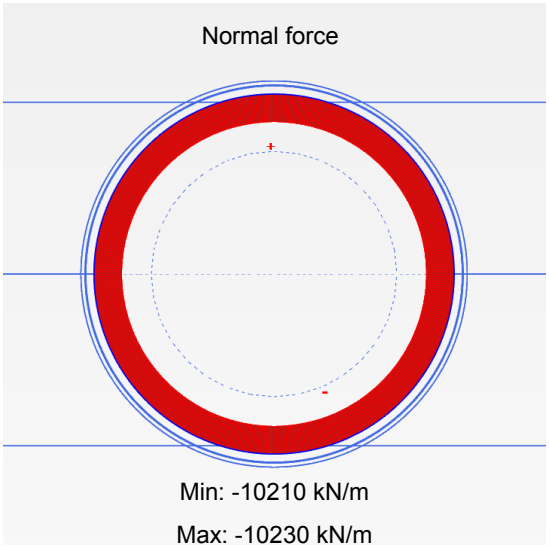

Fig. 30: Results for N_{max} and N_{min} scaled up by the factor 10^4.

	Calculation Section 1	Calculation Section 2
Normal force N	10230 kN/m	10220 kN/m
Displacements Pu_x	4,06 mm	4,06 mm

Tab. 8: Comparison of N and Pu_x for Calculation Section 1 and 2.

2.3.2.3 Evaluation of tunnel displacements on site

In order to decide on site whether the applied grouting pressure is adequate or has to be increased further the diametrical strains of the final lining are determined. Therefore, a mobile monitoring system was developed which permanently records the tunnel deformations.

Along the tunnel perimeter eight monitoring points are installed as shown in Figure 31.

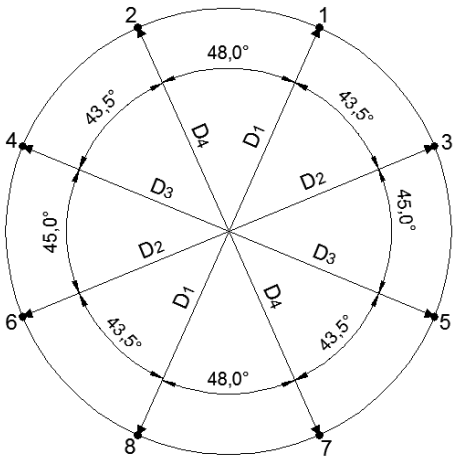

Fig. 31: Arrangement of monitoring points along the tunnel perimeter.

According to Figures 31 and 32 four different diameters D_1, D_2, D_3 and D_4 are measured before and after the interface grouting.

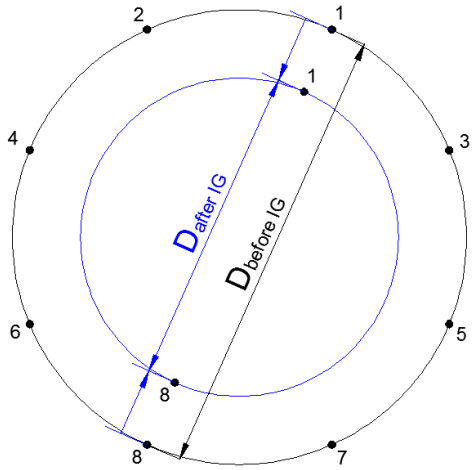

Fig. 32: Measuring of ΔD and calculation of ε_D on site.

Consequently, a mean value of ΔD is determined and the diametrical strain ε_D is calculated as follows:

$$\Delta D_i = D_{i,before\ IG} - D_{i,after\ IG} \qquad \textbf{Eq. 5}$$

i = 1, 2, 3, 4

$$\Delta D = \sum_{i=1}^{4} \frac{\Delta D_i}{4} \qquad \textbf{Eq. 6}$$

$$\varepsilon_D = \frac{\Delta D}{D_{inner}} \qquad \textbf{Eq. 7}$$

Where D_{inner} = 12600 mm.

2.3.2.4 Calculation of diametrical strains and comparison with the results measured on site

The calculation of the diametrical strains is carried out similar to the monitoring procedure on site. As demonstrated in Figure 33 ΔD is determined using the phase displacements |Pu| after the pressure application. In order to calculate the diametrical strain ΔD is referred to the initial internal diameter of the final lining (d_i = 12,6m = $D_{before\ IG}$).

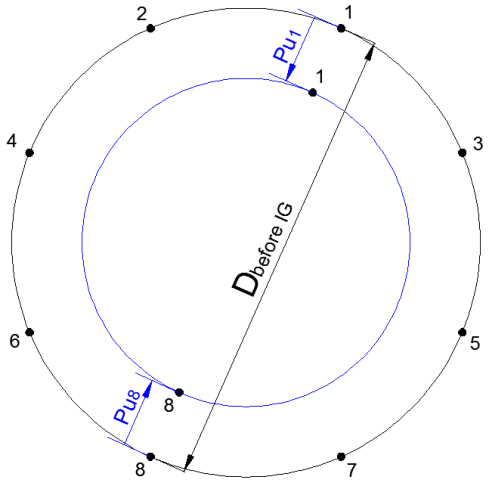

Fig. 33: Determination of ΔD and ε_D for the FE-calculation.

$$\Delta D = Pu_1 + Pu_8 \qquad \textbf{Eq. 8}$$

$$\varepsilon_D = \frac{\Delta D}{D_{before\ IG}} \qquad \textbf{Eq. 9}$$

A comparison of the calculated diametrical displacements for Calculation Section 1 and 2 with the results from the site is included in Table 9. Additionally, calculations are performed for different values of K_0.

		ΔD [mm]				ØΔD	ε_D
		1-8	3-6	4-5	2-7	[mm]	[-]
Displacements on site		-9,66	-3,73	-3,44	-6,43	-5,82	-4,6151E-04
Calculation Section 1	K_0 = 1,5	-8,19	-8,20	-8,20	-8,19	-8,20	-6,5041E-04
	K_0 = 2,5	-8,19	-8,20	-8,20	-8,19	-8,20	-6,5041E-04
Calculation Section 2	K_0 = 1,5	-8,19	-8,21	-8,21	-8,19	-8,20	-6,5041E-04
	K_0 = 3,5	-8,19	-8,21	-8,21	-8,19	-8,20	-6,5041E-04
	K_0 = 1-sin(φ)	-8,19	-8,21	-8,21	-8,19	-8,20	-6,5042E-04

Tab. 9: Comparison of diametrical displacements from the site with the FE-results.

From the comparison of the diametrical displacements in Table 9 it can be seen that ε_D is equal for Calculation Section 1 and 2. Additionally, the modification of K_0 does not influence the displacements of the final lining.

Furthermore, the obtained values for ΔD from the FE-analysis show that a constant pressure admission on the lining does not match the monitoring results from the site. Therefore, it is necessary to investigate an unsymmetrical pressure application in further detail.

2.4 Unsymmetrical pressure admission on the final lining

Calculation Section 2 is used to simulate the unsymmetrical pressure admission on the lining and K_0 is defined with 1,5.

2.4.1 Modelling of E_{gap} for unsymmetrical pressure application

The stiffness of the gap plays a pivotal role in order to successfully perform calculations using an unsymmetrical pressure admission which is demonstrated by means of the following results.

Figure 34 illustrates the pressure distribution in the gap clusters along the tunnel perimeter for the first calculation. While the left side of the tunnel is loaded with 7,5 bar the right side is loaded with 15 bar. In the first approach the gap stiffness is retained with 50 kPa along the entire tunnel perimeter.

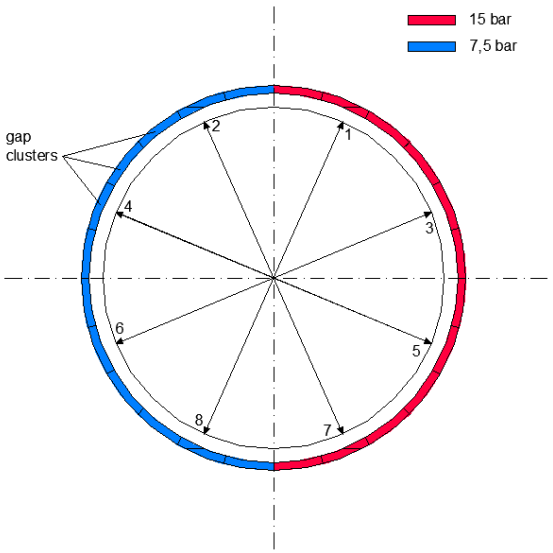

Fig. 34: Visualization of the pressure distribution with E_{gap} = 50 kPa.

Since the resulting force on the right hand side of the tunnel exceeds the one on the left side and due to the soft gap material the entire tunnel structure moves to the left when applying the pore pressure.

To avoid this numerical issue, the gap stiffness has to be varied along the tunnel perimeter. In a next step E_{gap} on the left half of the tunnel is kept to its original value of 15,0 GPa while E_{gap} on the right hand side is defined with 50 kPa. As shown in Figure 35 the applied pressure is zero on the left side and 15 bar on the right half. The results presented in Figure 36 show that the pressure application succeeds.

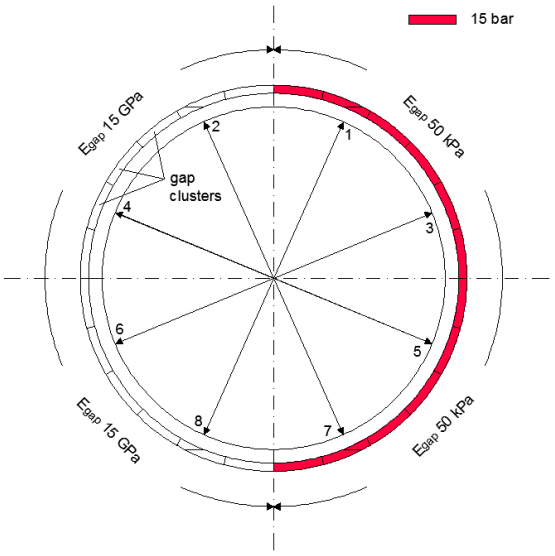

Fig. 35: Left tunnel half: 0bar, E_{gap} = 15 GPa. Right tunnel half: 15bar, E_{gap} = 50 kPa.

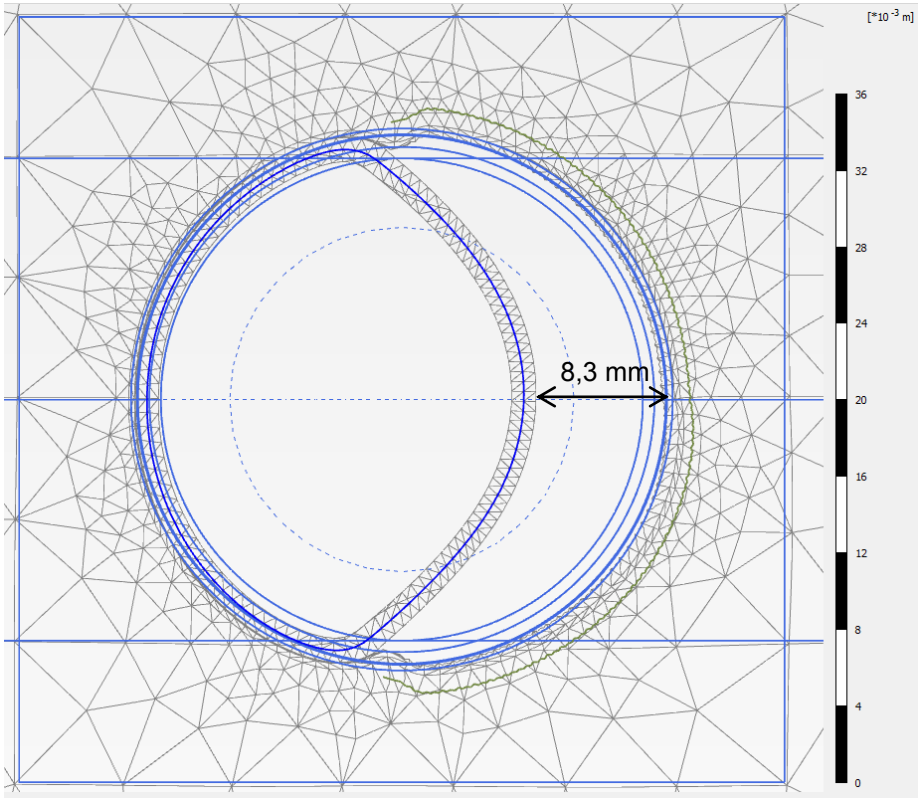

Fig. 36: Deformed mesh for pressure admission as illustrated in Fig. 35.

2.4.2 Specification of Variation 1 and Variation 2

According to the experiences gained on site the tunnel lining is primarily pre-stressed under a constant pressure distribution of 8 bar. After the hardening of the grout the injection is repeated in a second pressure phase to increase the pre-stressing pressure of the final lining.

As illustrated in Figure 37 on site the injection procedure in the second pressure phase starts at the walls of the tunnel. Basically, the pre-stressing is separated into the injection of the top and the injection of the invert.

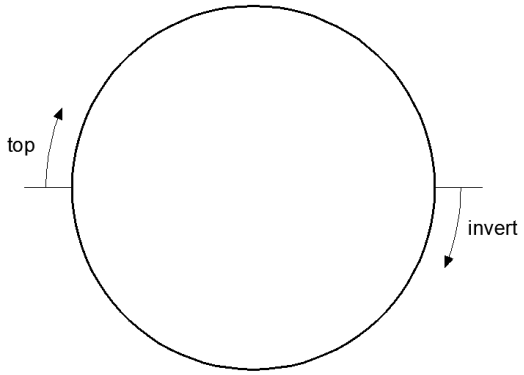

Fig. 37: Visualization of the injection procedure on site for Pressure Phase 2.

The highest pressures in phase 2 are estimated to occur at the walls where the injection process starts. As the grout proceeds along the tunnel perimeter the pressure slowly decreases and reaches a minimum when arriving at the opposite wall. The hardened grout of phase 1 is assumed to fracture where the original pre-stressing pressure of 8 bar is exceeded. Consequently the gap stiffness is zero in the fractured zones. To account for this in the FE-calculation the gap stiffness is defined with a low value where 8 bar are exceeded in the second phase. If the pressure keeps 8 bar in the second phase a high gap stiffness is defined since fracturing does not occur.

In the following two different load cases are analyzed for the unsymmetrical pressure application in Pressure Phase 2. In Variation 1 (Figure 38) a pressure distribution has to be found in order to generate similar diametrical displacements as measured on site. The monitored displacements are given in Table 11.

Variation 2 (Figure 38) simulates the reverse case where the pressure distribution is known and the diametrical displacements have to be calculated. In this case the pressure distribution is defined according to a rough estimation obtained from the site.

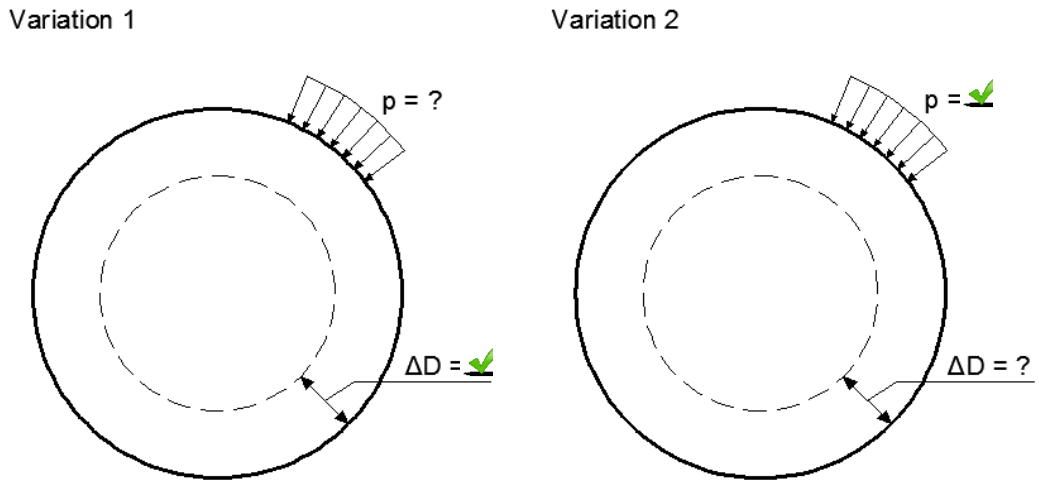

Fig. 38: Comparison of Variation 1 and 2.

At the beginning the calculation phases have to be modified for both presented variations. After the activation of the final lining a constant pressure distribution is applied on the lining in Pressure Phase 1. Afterwards the applied pressure is increased but distributed unsymmetrically along the tunnel perimeter. According to measurements on site the maximum pre-stressing pressure is estimated between 11 and 12 bar. The updated Calculation phases are included in Table 10.

Phase	Comments
0. Initial phase	K_0 = 1,5
1. Excavation	M_{stage} = 0,2
2. Activation shotcrete	M_{stage} = 1,0
3. Activation gap material & final lining	E_{gap} = 15,0 GPa
4. Pressure Phase 1	p = 8 bar constant, E_{gap} = 50 kPa. Reset displacements to zero.
5. Pressure Phase 2	p = unsymmetrical, E_{gap} = variable

Tab. 10: Updated calculation phases for unsymmetrical pressure admission.

2.4.2.1 Results for Variation 1

Figure 39 shows the required pressure distribution in Pressure Phase 2 in order to obtain similar diametrical displacements as measured on site. While the maximum pressure of 11,5 bar occurs in the top and invert of the tunnel the minimum pressure is

applied at the walls. The gap stiffness is increased to 15 GPa at the walls in Pressure Phase 2.

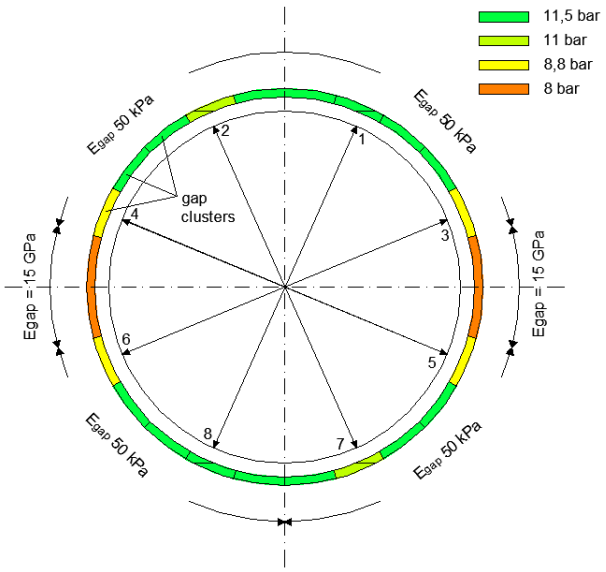

Fig. 39: Pressure distribution in Pressure Phase 2.

Furthermore, the resulting lining displacements from Pressure Phase 2 are presented in Figure 40.

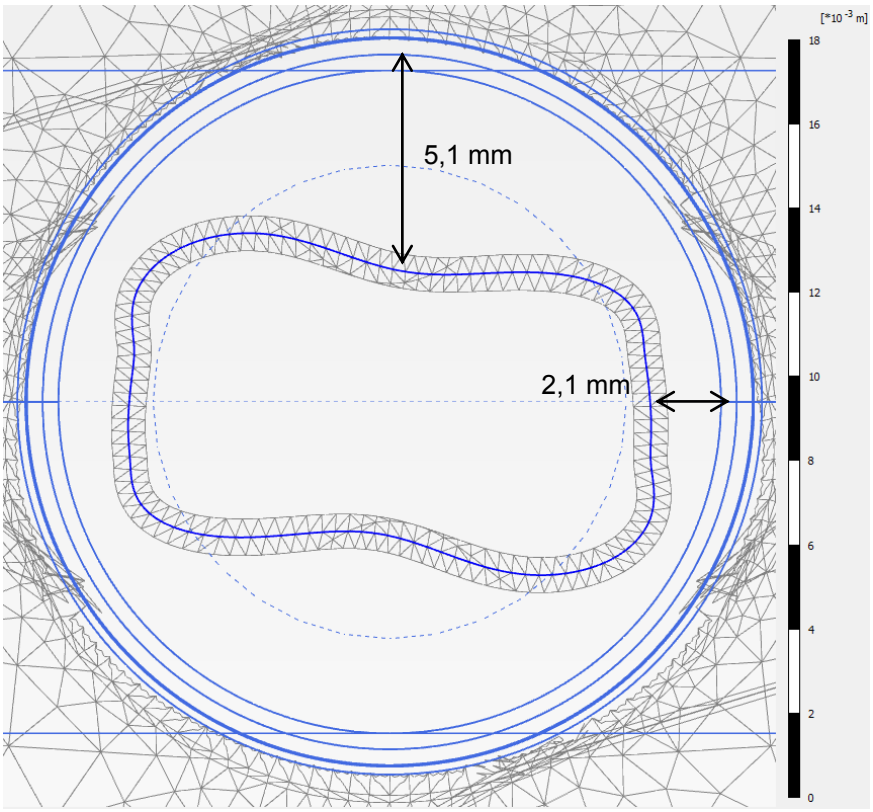

Fig. 40: Total displacements |u| for Pressure Phase 2.

2.4.2.2 Results for Variation 2

Figure 41 illustrates the pressure distribution in Pressure Phase 2. The maximum pressure of 11 bar occurs at the walls where the grout is injected. E_{gap} is increased to 15 GPa as demonstrated in Figure 41. The resulting deformations of the lining can be found in Figure 42.

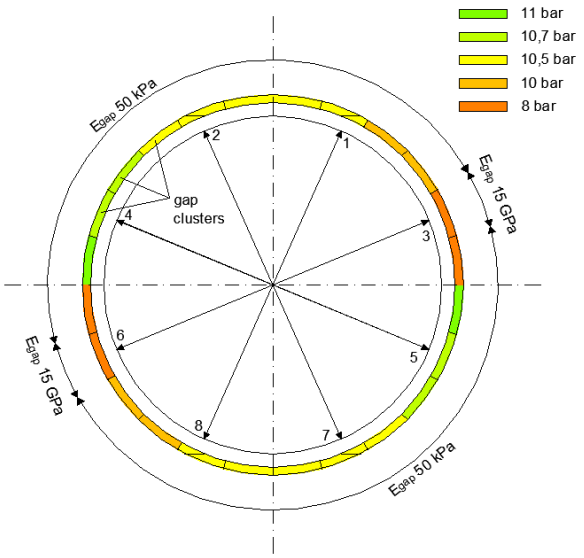

Fig. 41: Pressure distribution in Pressure Phase 2.

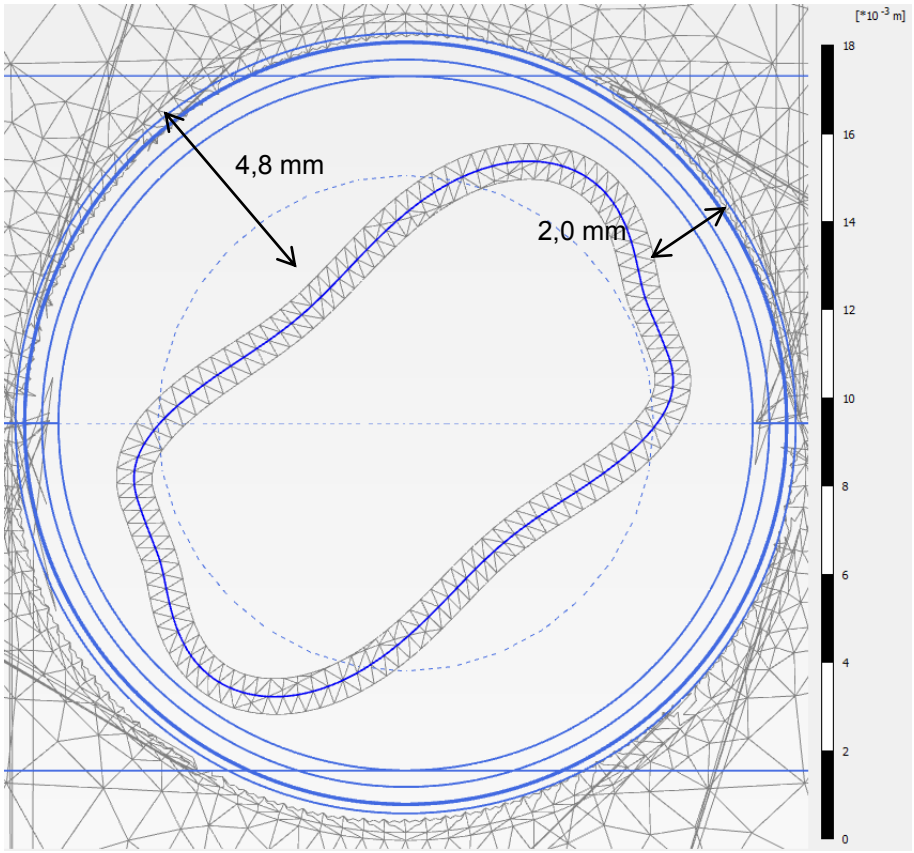

Fig. 42: Total displacements |u| for Pressure Phase 2.

The evaluated diametrical displacements from the site as well as for Variation 1 and 2 are given in Table 11.

	ΔD [mm]				ØΔD	ε_D
	1-8	3-6	4-5	2-7	[mm]	[-]
Displacements on site	-9,66	-3,73	-3,44	-6,43	-5,82	-4,6151E-04
Variation 1	-9,60	-3,92	-3,45	-6,79	-5,94	-4,7139E-04
Variation 2	-2,68	-4,13	-8,22	-8,33	-5,84	-4,6363E-04

Tab. 11: Diametrical displacements of Variation 1 and 2 and the monitored results on site.

2.5 Application of the Hoek-Brown material model

So far all calculations have been performed with the Mohr-Coulomb model. In this chapter the Hoek-Brown model is used and the results are compared to the Mohr-Coulomb calculations.

2.5.1 The Hoek-Brown Criterion

The Hoek-Brown Criterion is defined by the following equation [4]:

$$\sigma_1 = \sigma_3 + \sigma_{ci}\left(m_b \frac{\sigma_3}{\sigma_{ci}} + s\right)^a \qquad \textbf{Eq. 10}$$

where σ_{ci} is the uniaxial compressive strength of the intact rock and s, a and m_b are model constants. In order to calculate the model constants the following Hoek-Brown parameters are required:

σ_{ci} … uniaxial compressive strength of the intact rock [MPa]

GSI … geological strength index [-]

m_i … rock mass constant for intact rock [-]

D … disturbance factor for rock masses [-]

The factor D quantifies the disturbance of the rock and varies from 0 for undisturbed to 1 for disturbed rock masses. The relationships between the GSI and the model constants are as follows [4]:

$$m_b = m_i exp\left(\frac{GSI-100}{28-14D}\right) \quad \textbf{Eq. 11}$$

$$s = exp\left(\frac{GSI-100}{9-3D}\right) \quad \textbf{Eq. 12}$$

$$a = \frac{1}{2} + \frac{1}{6}\left(\exp\left(-\frac{GSI}{15}\right) - \exp(-\frac{20}{3})\right) \quad \textbf{Eq. 13}$$

Figure 43 illustrates the Hoek-Brown failure curve for the Queenston Q10 material plotted in a $\sigma_1 - \sigma_3$ diagram. The required Hoek-Brown parameters are given in Appendix (5).

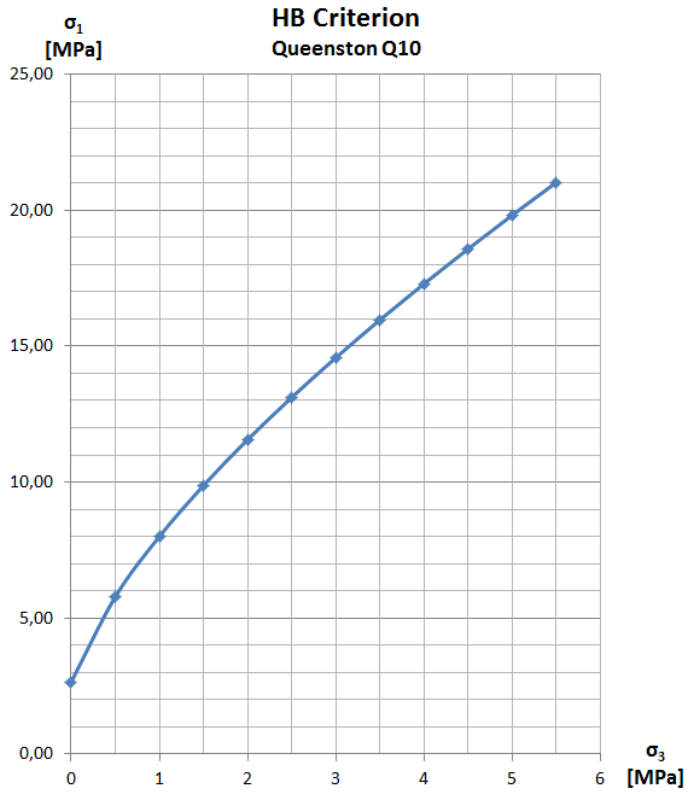

Fig. 43: Hoek-Brown criterion for the Queenston Q10 layer.

2.5.2 Calculation of equivalent Mohr-Coulomb parameters

Different methods can be applied to calculate equivalent cohesion and friction angle from Hoek-Brown parameters. On the one hand, c' and φ' can be calculated by fitting the MC-line tangentially to the HB-failure curve at a specific minor principal stress. On

the other hand, a regression method over a dominant stress range can be applied to evaluate c' and φ' [6]. The second method is most frequently used and therefore, applied in the following chapters.

2.5.2.1 Regression method [6]

Using the regression method a linear relationship is applied in order to fit the HB-failure line. Therefore, the equivalent MC-parameters are calculated as follows:

$$\varphi' = sin^{-1}\left[\frac{6am_b(s+m_b\sigma'_{3n})^{a-1}}{2(1+a)(2+a)+6am_b(s+m_b\sigma'_{3n})^{a-1}}\right] \quad \textbf{Eq. 14}$$

$$c' = \frac{\sigma_{ci}\left[(1+2a)s+(1-a)m_b\sigma'_{3n}\right](s+m_b\sigma'_{3n})^{(a-1)}}{(1+a)(2+a)\sqrt{1+(6am_b(s+m_b\sigma'_{3n})^{a-1})/((1+a)(2+a))}} \quad \textbf{Eq. 15}$$

where

$$\sigma'_{3n} = \frac{\sigma'_{3max}}{\sigma_{ci}} \quad \textbf{Eq. 16}$$

σ'_{3max} has to be determined for each case individually. In the following two different ways are presented to calculate σ'_{3max}.

Alternative 1:

For general geotechnical applications it is supposed to calculate σ'_{3max} as [5]:

$$\sigma'_{3max} = 0{,}25 * \sigma_{ci} \quad \textbf{Eq. 17}$$

Alternative 2:

For shallow and deep tunnel applications σ'_{3max} can be determined according to the following formula [4]:

$$\sigma'_{3max} = \sigma'_{cm} * 0{,}47\left(\frac{\sigma'_{cm}}{\gamma H}\right)^{-0{,}94} \quad \textbf{Eq. 18}$$

where

$$\sigma'_{cm} = \sigma_{ci} * \frac{(m_b+4s-a(m_b-8s))(\frac{m_b}{4}+s)^{(a-1)}}{2(1+a)(2+a)} \quad \textbf{Eq. 19}$$

σ'_{cm} represents the global rock mass strength. Additionally, the tunnel depth H below the surface as well as the unit weight of the rock material γ is taken into account in Alternative 2.

The equivalent MC-parameters are calculated for the Queenston Q10 material, using Alternative 1 and 2 in order to calculate σ'_{3max}. In the next step the resulting strength parameters c' and φ' have to be transformed into the $\sigma_1 - \sigma_3$ diagram. Therefore, the following formula is applied [7]:

$$\sigma'_1 = \frac{2c'\cos\varphi'}{1-sin\varphi'} + \frac{1+sin\varphi'}{1-sin\varphi'}\sigma'_3 \qquad \textbf{Eq. 20}$$

The results for Alternative 1 and 2 are compared in Figure 44.

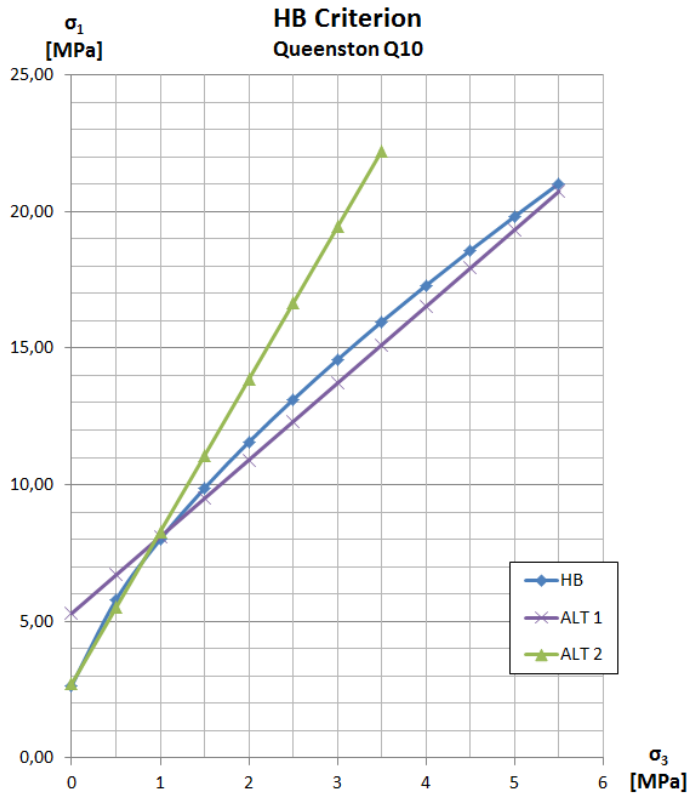

Fig. 44: Comparison of Alternative 1 with Alternative 2 for the Queenston Q10.

From Figure 44 it can be seen that Alternative 2 instead of Alternative 1 is to be preferred for σ_3 < 1MPa and vice versa for σ_3 > 1MPa.

2.5.2.2 Fitting of the HB-curve with given MC-parameters

The design report [1] provides HB-parameters as well as MC-parameters for every rock material given in the longitudinal section. The aim of this chapter is to find out if the

MC-parameters fit the HB-parameters in the $\sigma_1 - \sigma_3$ diagram. The investigations are performed for the Queenston Q10 and the Whirlpool formation.

At Calculation Section 2 σ_3 in the initial phase is approximately 2 MPa at the elevation of the tunnel axis. It is expected that the evaluated MC-line matches with the HB-failure curve around σ_3 = 2 MPa.

In the first step the HB-failure curves are developed for the Queenston Q10 and Whirlpool using the given HB-parameters from the design report [1]. Afterwards the known MC-parameters for both materials are transferred into $\sigma_1 - \sigma_3$ diagram according to Eq. 20. The results are illustrated in Figures 45 and 46.

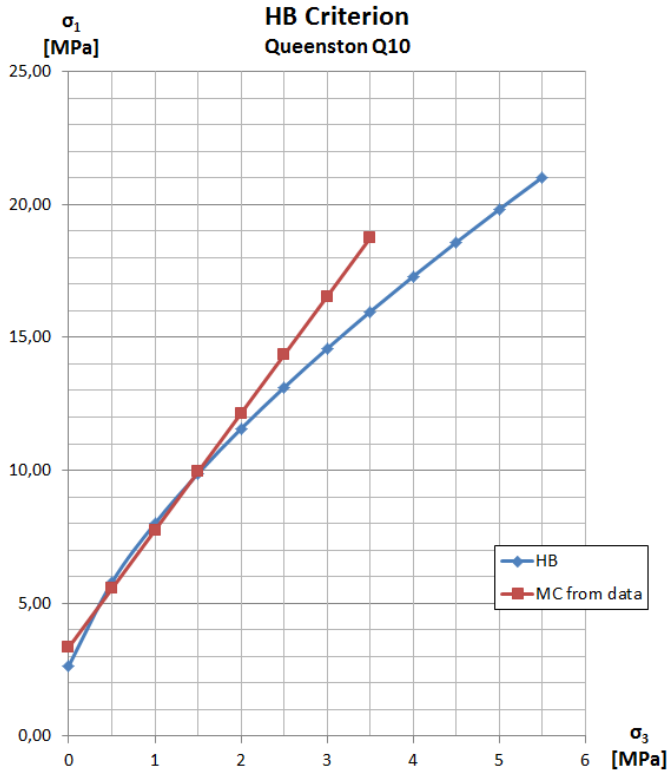

Fig. 45: Comparison of HB-curve and MC-line for Queenston Q10.

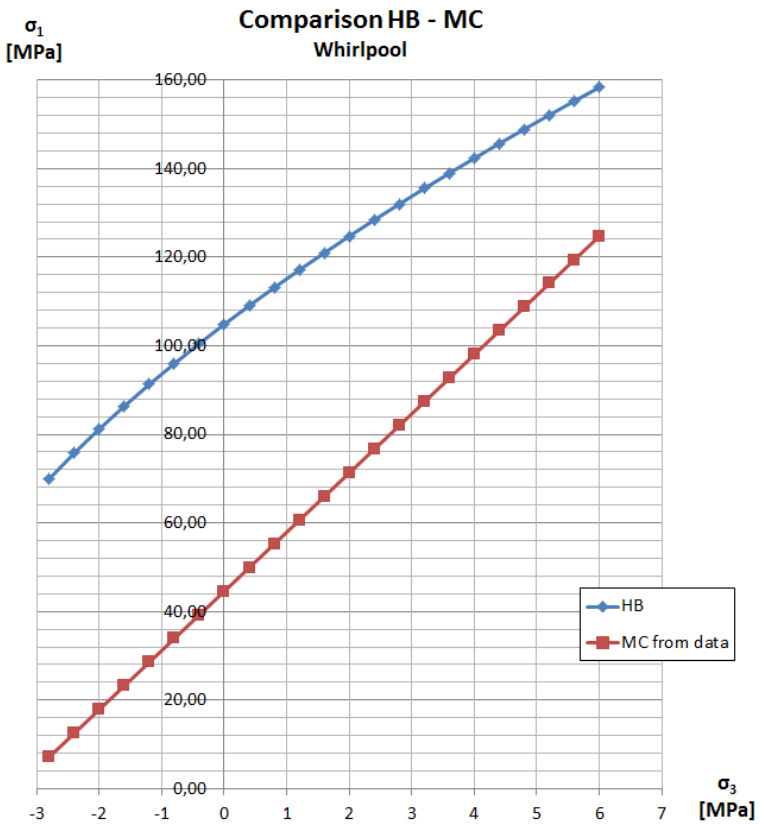

Fig. 46: Comparison of HB-curve and MC-line for Whirlpool.

As illustrated in Figure 45 the MC-line obtained from the given c' and φ' for the Queenston Q10 fits the HB-curve at least for σ_3 < 3 MPa. From the results in Figure 46 it can be concluded that the MC-line for the Whirlpool formation does not fit the HB-curve for any values of σ_3.

2.5.3 Comparison of displacements for MC and HB

In this chapter the pre-stressing of the final lining is performed using the HB-model in order to describe the material behaviour of the rock. The calculations are executed for Calculation Section 2 using the same calculation phases as given in Table 10. A pressure distribution as illustrated in Figure 39 is applied on the final lining in Pressure Phase 2. The HB-parameters for the different rock formations can be found in Appendix (5).

A comparison of the deformed mesh for the MC-model with the HB-model is demonstrated in Figures 47 and 48 with the results for the activation of the shotcrete.

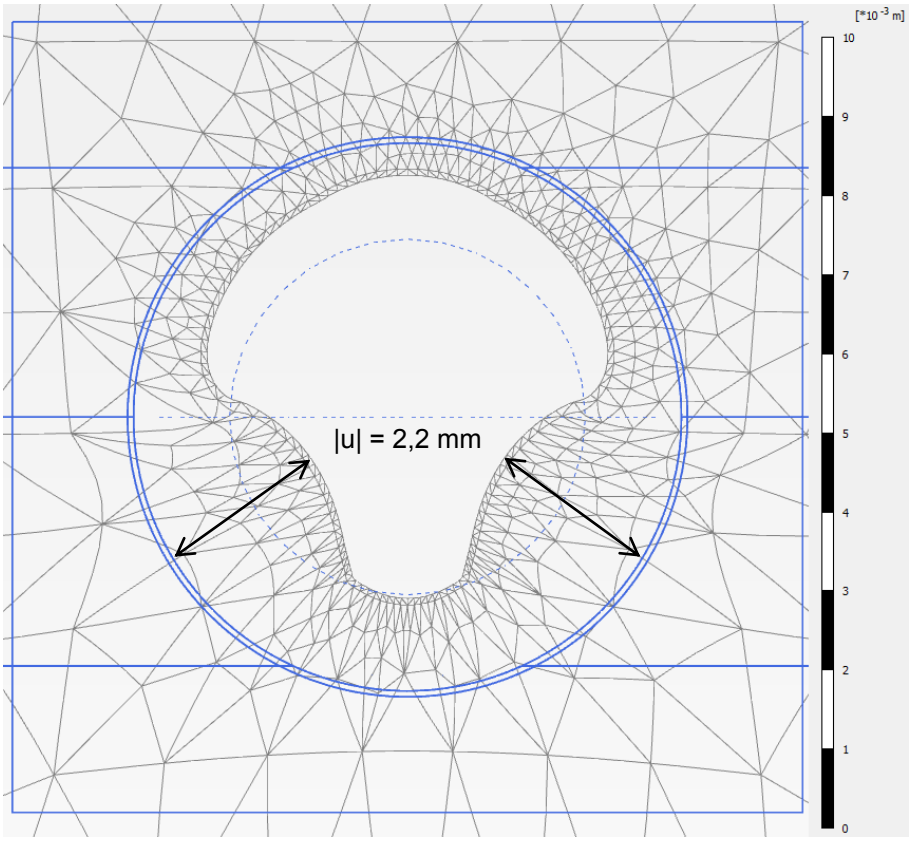

Fig. 47: Deformed mesh for the activation of the shotcrete when using the MC-model.

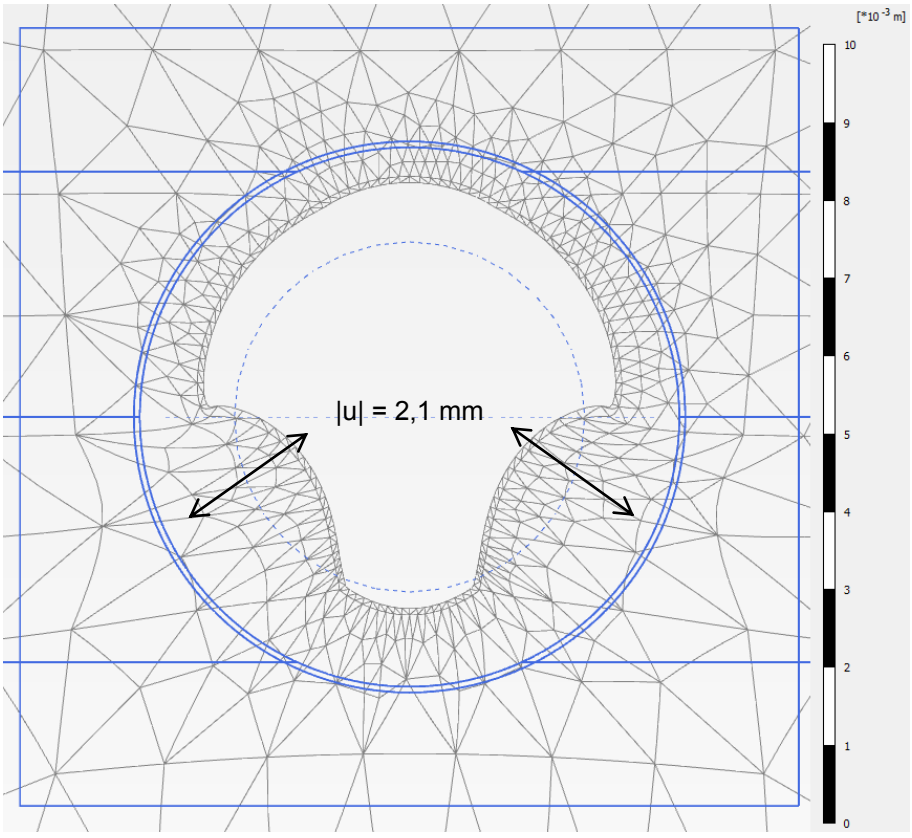

Fig. 48: Deformed mesh for the activation of the shotcrete when using the HB-model.

Furthermore, the diametrical strains after the pressure application in Pressure Phase 2 are evaluated for the HB-model and the results are compared in Table 12 with the results for the MC-model.

	ΔD [mm]				ØΔD	ε_D
	1-8	3-6	4-5	2-7	[mm]	[-]
MC	-9,60	-3,92	-3,45	-6,79	-5,94	-4,7139E-04
HB	-9,60	-3,92	-3,45	-6,79	-5,94	-4,7141E-04

Tab. 12: Comparison of diametrical strains for the MC-model with the HB-model.

Figures 47 and 48 demonstrate that the difference in the tunnel deformations for the MC- and the HB-model are negligible. As illustrated in Table 12 the diametrical strains of the lining are not affected when changing the MC- parameters to HB-parameters.

2.6 Seeber-diagrams

In this chapter a Seeber-diagram is developed on the basis of the results obtained from the FE-calculation and compared with the results on site. Furthermore, the influence of plastic rock behaviour on the diametrical displacements during pre-stressing and watering-up is investigated.

2.6.1 Introduction [2]

In general, the Seeber-diagram is set up for the resulting forces in the gap between the lining and the rock material as illustrated in Figure 49. In case of the analyzed tunnel the gap occurs between the final lining and the shotcrete.

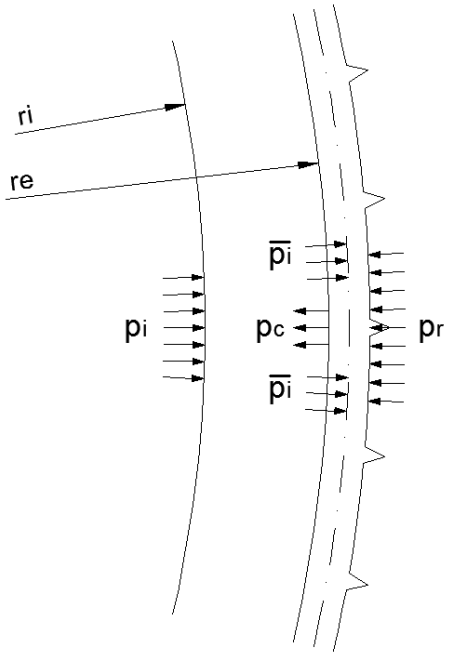

Fig. 49: Applying p_i to the gap and general specification of $\overline{p_\iota}$.

Since the internal water pressure p_i is applied at the inside of the final lining it has to be referred to the gap. This is carried out by the following approximation:

$$\overline{p_\iota} = p_i * \frac{r_i}{r_e} \qquad \textbf{Eq. 21}$$

In the following three different examples are set up to demonstrate the principal approach of the Seeber-diagram.

The Seeber-diagram includes a characteristic line for the concrete and the rock material. While the characteristic line of the rock material is depending on the Young's modulus, the concrete line is a function the Young's modulus and the thickness of the lining.

As illustrated in Figure 50 the pressure (p_R, p_c) is plotted versus the radial strain $\varepsilon(r_e)$. Since pressures and strains are related to the gap, the outer strain of the concrete lining $\varepsilon(r_e)$ has to be considered to set up the Seeber-diagram correctly.

In a first approach pre-stressing is not taken into account. As demonstrated in Figure 50 the characteristic line of the rock material is plotted in the first quadrant and the concrete line is drawn in the 4th quadrant. The applicable internal pressure is restricted by the maximum tensile strain (max ε_{tc}) in the concrete lining. As illustrated in Figure 50 $\overline{p}_{i,1}$can be split up into $p_{R,1}$ and $p_{C,1}$. Since max ε_{tc} is small for unreinforced concrete

and tension in the concrete is generally to be avoided the results of Example 1 are not satisfying.

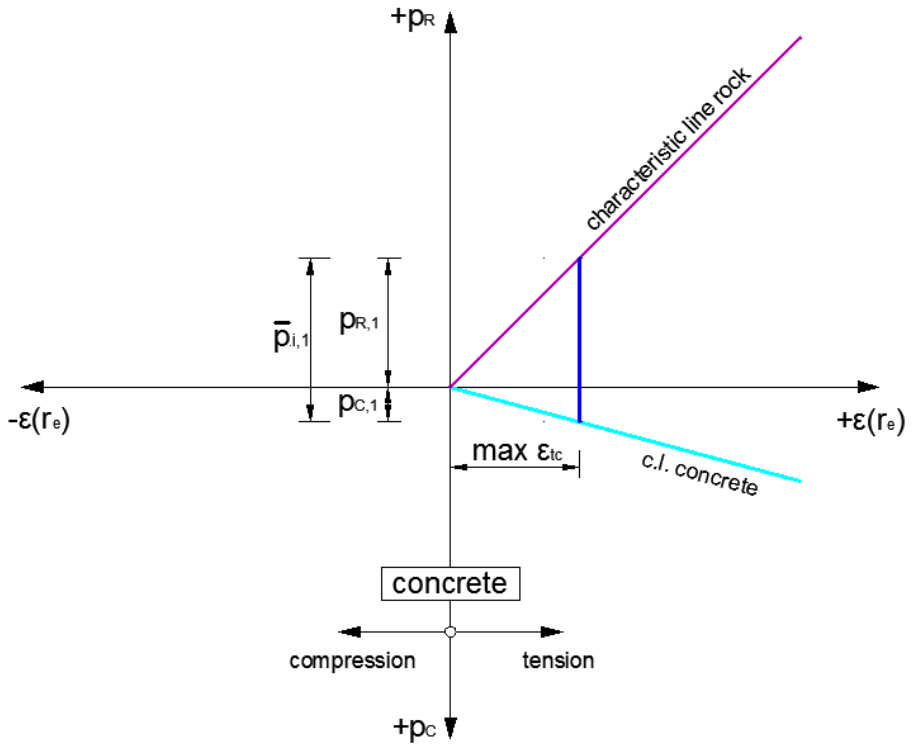

Fig. 50: Example 1. Tension in the lining since pre-stressing pressure = 0.

In order to avoid tension in the concrete lining pre-stressing is required. Therefore, the concrete line is extended into the second quadrant as demonstrated in Figure 51. The maximum compression strain of the concrete max ε_{cc} is assigned on the x-axis. The corresponding y-coordinate on the concrete lining defines the maximum applicable pre-stressing pressure (Point 1). Furthermore, the characteristic line of the rock is moved to Point 1. Additionally, the rock strain ε_R which results from the pre-stressing can be determined on the x-axis. With ε_R and max ε_{cc} the size of the gap opened during the injection can be determined. Assuming that tension in the concrete lining has to be avoided the maximum applicable internal water pressure $\bar{p}_{i,2}$ is illustrated in Figure 51.

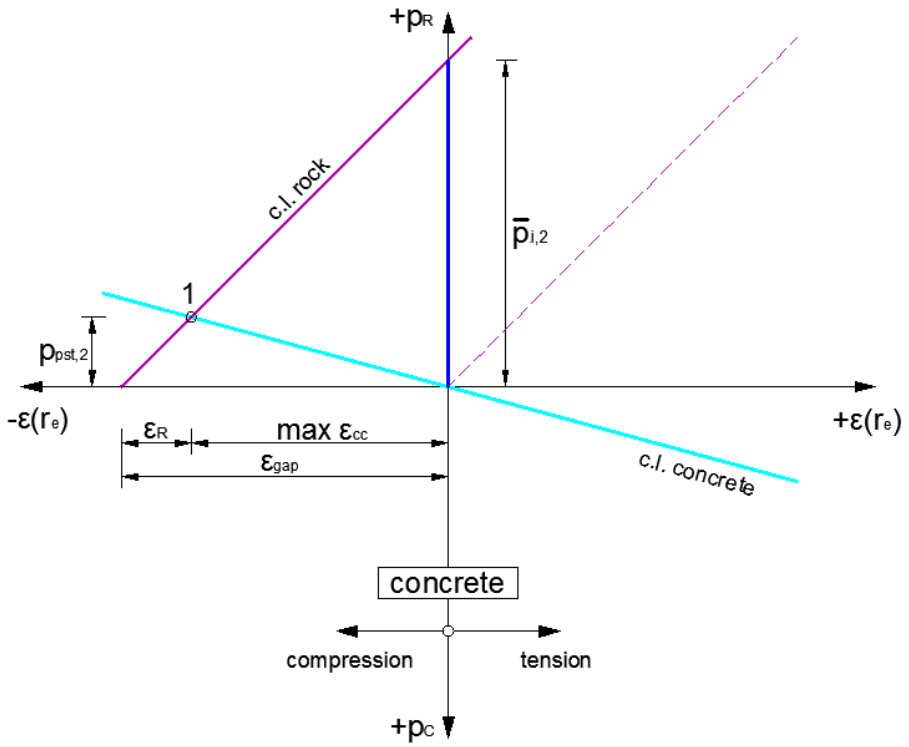

Fig. 51: Example 2. $P_{pst,2}$ = pre-stressing pressure. $\bar{p}_{i,2} > \bar{p}_{i,1}$ due to pre-stressing.

In practice, the initially applied pre-stressing pressure reduces due to creep of the concrete and temperature decrease when watering up the tunnel. Figure 52 demonstrates how losses of the pre-stressing pressure are considered in the Seeber-diagram. The initial $p_{pst,2}$ is reduced to a remaining pressure $p_{pst,3}$. Consequently, the maximum applicable internal water pressure decreases. The remaining rock strain ε_R and concrete strain ε_c can be determined on the x-axis.

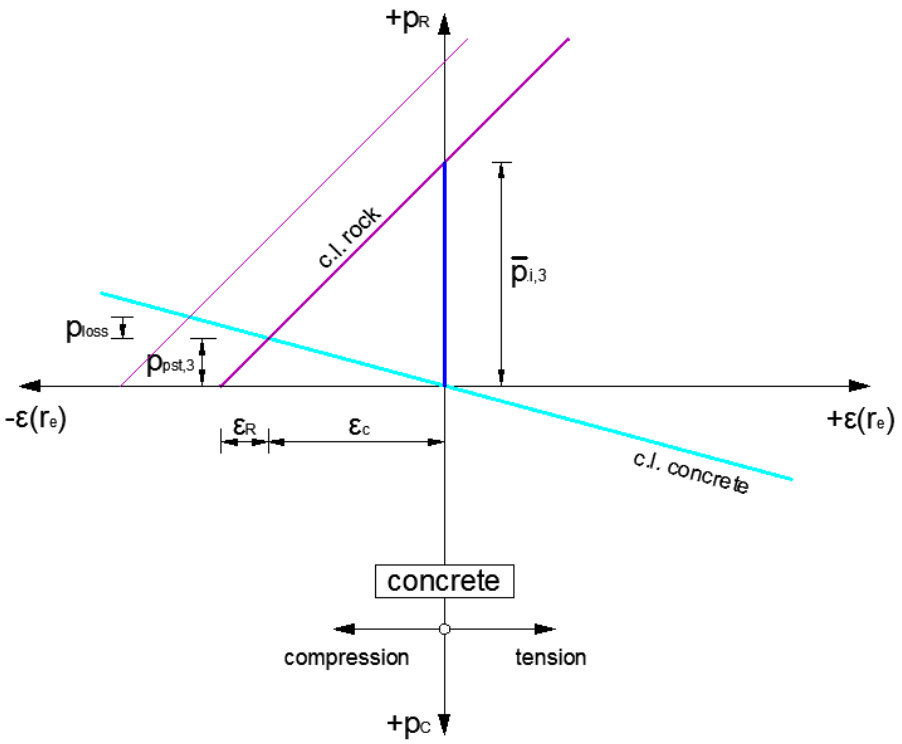

Fig. 52: Example 3. Accounting for losses. $\bar{p}_{i,2} > \bar{p}_{i,3}$.

2.6.2 Seeber-diagram based on site measurements

With the monitored displacements of the final lining a Seeber-diagram is developed. The results are illustrated in Figure 53. The pressure (pre-stressing and internal pressure) is plotted on the y-axis and the radial strains of the concrete and rock material are plotted on the x-axis. Initially the final lining is pre-stressed with 11,1 bar which is specified as short-term pressure (p_{st}). For this pressure the characteristic lines of the concrete and rock are developed on site. The corresponding strains in Point 1 are defined as $\varepsilon_{R,1}$ and $\varepsilon_{c,1}$. Due to losses (creep, temperature decrease) the initial pre-stressing pressure reduces to p_{lt} (long-term pressure) which is the minimum required pressure in order to guarantee a long-term stability of the structure. The corresponding strains in Point 2 are specified as $\varepsilon_{R,2}$ and $\varepsilon_{c,2}$. Finally, an internal water pressure $\bar{p}_i$ of 5 bar is applied on the final lining due to the watering-up. The resulting strains in the rock and concrete have to be determined graphically. This is carried out by inserting $\bar{p}_i$ between the rock line and the rock line as illustrated in Figure 53. Due to $\bar{p}_i$ the rock strains are further increased while the strains in the concrete are decreased. The resulting strains $\varepsilon_{R,w}$ and $\varepsilon_{c,w}$ after watering-up are demonstrated in Figure 55.

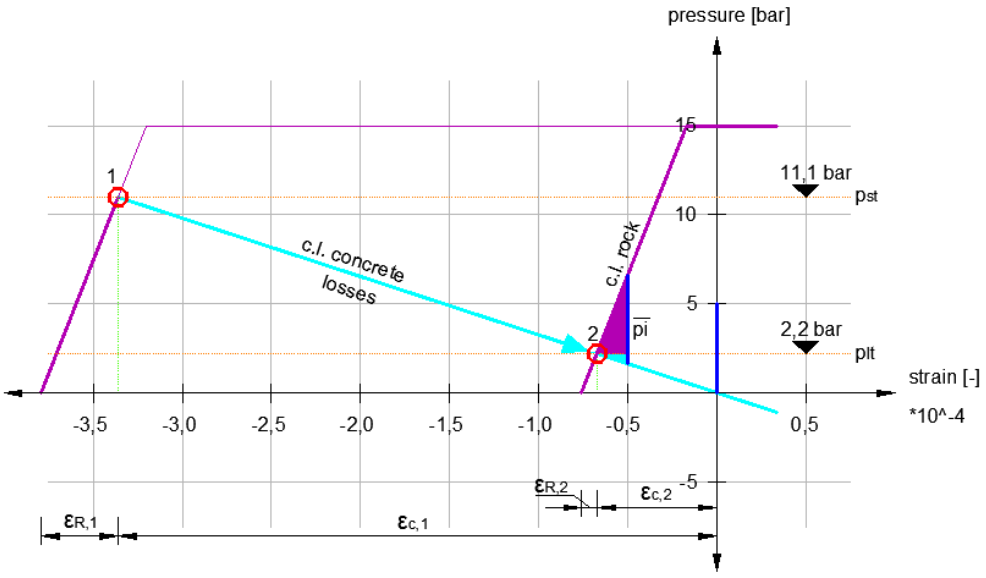

Fig. 53: Seeber-diagram developed on site.

Table 15 includes the resulting rock and concrete strains for each phase of the Seeber-diagram.

2.6.3 Development of Seeber-diagram based on the FE-results and comparison with the results on site

2.6.3.1 Seeber-diagram for the calculations with MC-model

In a first approach the results for the MC-model are used to develop the Seeber-diagram.

Primarily the calculation phases have to be adopted and extended. According to the Seeber-diagram developed on site, the initial pre-stressing pressure is 11,1 bar along the entire tunnel perimeter. For the correct evaluation of the diametrical strains, the displacements are set to zero in this phase. Afterwards, the pressure has to be released to 2,2bar in order to account for losses. During the two pressure phases E_{gap} is defined with 50 kPa. In the next phase the gap stiffness is increased to 15,0 GPa.

As illustrated in Figure 55 $\bar{p}_i$ is 5bar. The internal water pressure is applied by activating the pore pressure in the clusters of the tunnel interior. According to Eq. 21 p_i is calculated as follows:

$$p_i = \frac{6{,}9\ m}{6{,}3\ m} * 5{,}0\ bar = 5{,}5 bar$$

The internal water pressure p_i is applied in the last phase. The adopted calculation phases for the Seeber-diagram are given in Table 13.

Phase	Comments
0. Initial phase	K_0 = 1,5
1. Excavation	M_{stage} = 0,2
2. Activation shotcrete	M_{stage} = 1,0
3. Activation gap material & final lining	E_{gap} = 15,0 GPa
4. Pressure phase	p = 11,1bar constant. Reset displacements to 0, E_{gap} <<
5. Pressure release	p = 2,2 bar to account for losses.
6. Exchange E_{gap}	p = 2,2 bar, E_{gap} >>
7. Internal water pressure	p_i = 5,5 bar.

Tab. 13: Calculation phases for the Seeber-diagram.

The calculation of the strains for the Seeber-diagram is carried out as described in Chapters 2.3.2.3 and 2.3.2.4. Therefore, the diametrical concrete strain ε_c is determined for the outer diameter of the final lining (D= 13 800mm) and the diametrical rock strain ε_R is calculated for the tunnel diameter after the excavation (D= 14 160mm).

As an example the calculation of ε_c and ε_R is illustrated in Appendix (7) and (8) for the pressure phase (p = 11,1 bar).

In Figure 54 the Seeber-diagram based on the site results is compared with the FE-results. The latter are represented by the dashed lines. The divergence of the concrete lines can be explained by the fact that the thickness of the final lining is usually larger than 60 cm on site. Conclusively, the concrete line developed on site is steeper. The results for the rock and concrete strains in Point 2 and Point 2' can be found in Table 15.

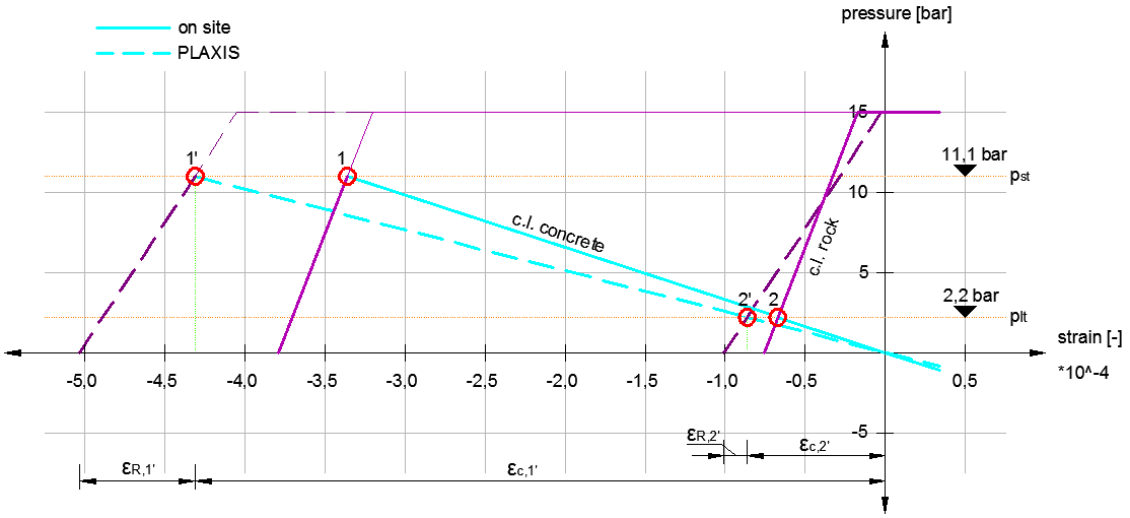

Fig. 54: Comparison of Seeber-diagram developed on site with the FE-results.

Figures 55 and 56 demonstrate a detailed view of the Seeber-diagrams for the watering-up phase. Figure 55 present the results developed on site and Figure 56 illustrates the results from the FE-analysis.

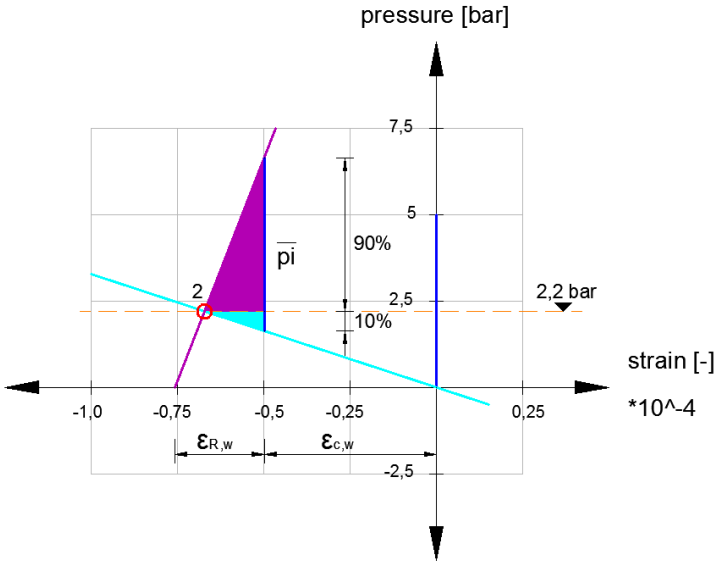

Fig. 55: Seeber-diagram developed on site for the watering-up.

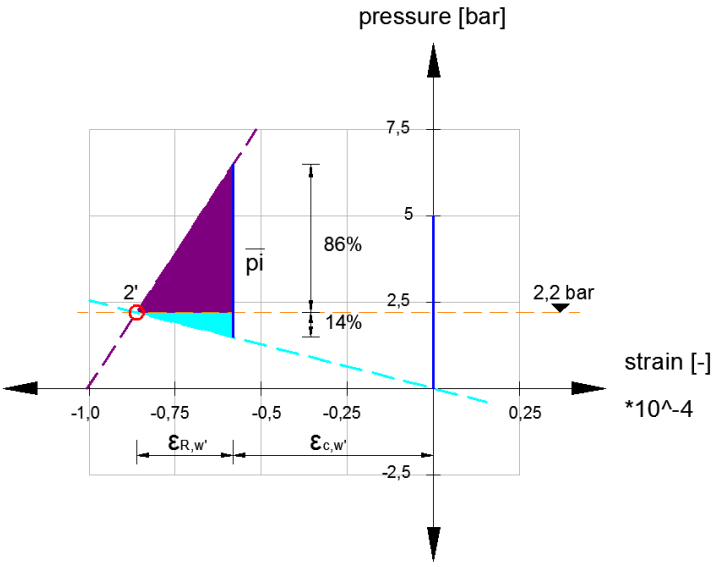

Fig. 56: Seeber-diagram developed with FE-results for the watering-up.

According to Figures 55 and 56 it can be seen that from the site measurements the rock material is estimated to sustain 90% of the internal water pressure while the FE-results predict 86%.

2.6.3.2 Diametrical strains for reduced UCS

When analysing the plastic points of the FE-calculation it can be found that no plastic points occur in the phases 4 to 7 (Table 13). Therefore, the material behaviour of the rock is elastic during the pressure phases. This is the case for the given MC- and HB-parameters.

In an additional study the influence of plastic rock behaviour on the results in the Seeber-diagram is investigated. Therefore, the UCS of four different rock materials (Power Glen, Whirlpool, Queenston Q10 and Queenston Q6-Q9) is reduced. Two different calculations are performed which are specified in Table 14.

UCS [MPa]	Original	Calculation 1	Calculation 2
Power Glen	172	26	26
Whirlpool	216	63	0,3
Queenston Q10	33	10	10
Queenston Q9-Q6	33	8	8

Tab. 14: Reduced UCS parameters for Calculation 1 and Calculation 2.

The plastic points for Calculation 1 and 2 are presented in Figures 57 to 60.

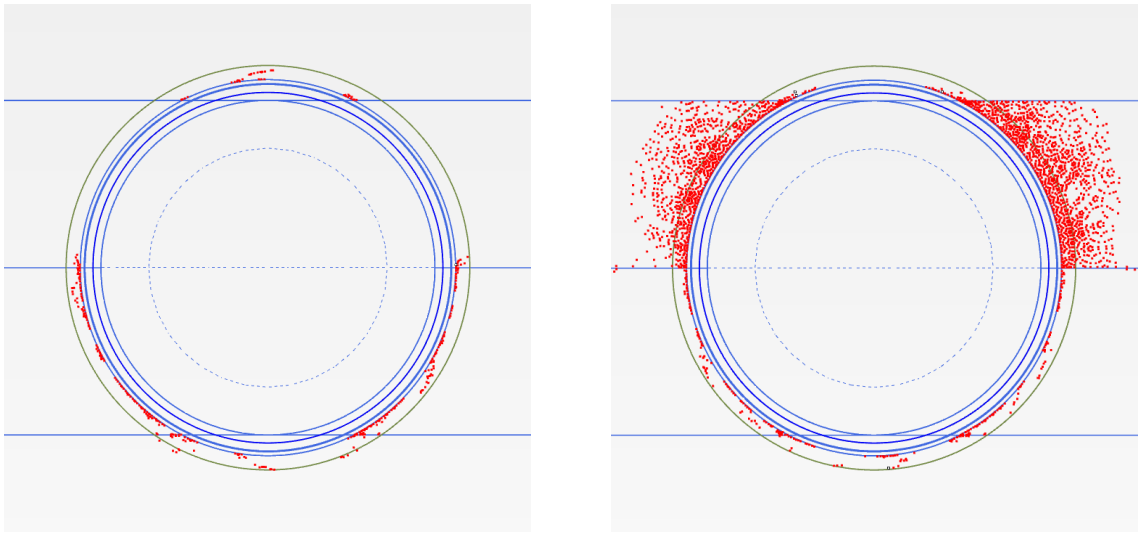

Fig. 57: Plastic points for the pressure phase: Calculation 1 (left) and Calculation 2 (right).

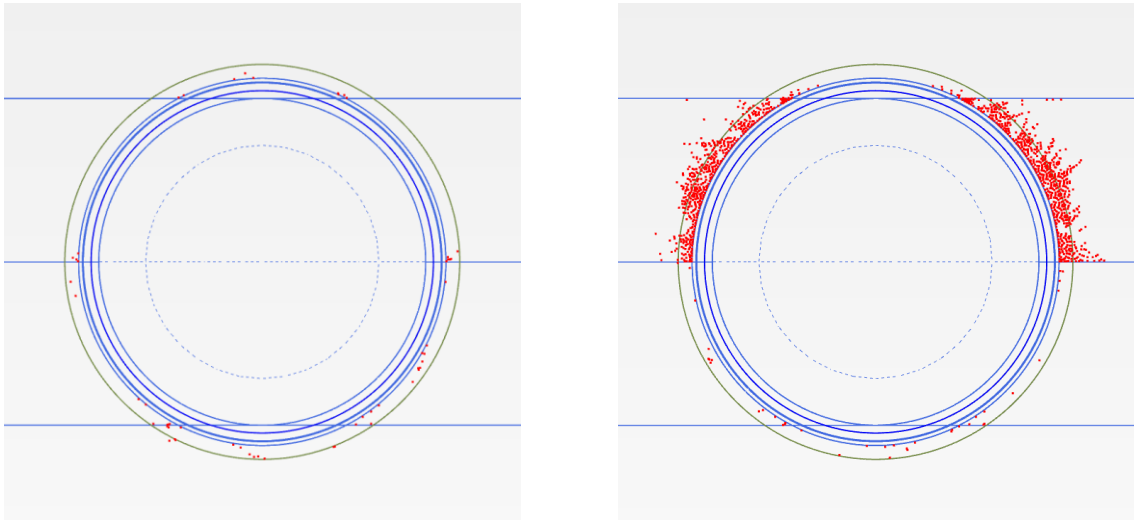

Fig. 58: Plastic points for the pressure release: Calculation 1 (left) and Calculation 2 (right).

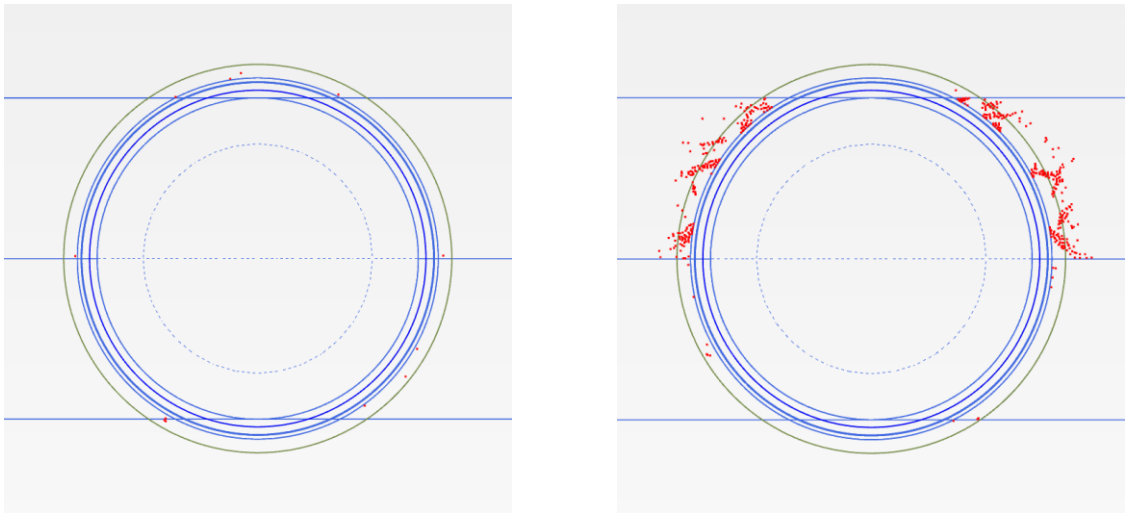

Fig. 59: Plastic points for the exchange of E_{gap}: Calculation 1 (left) and Calculation 2 (right).

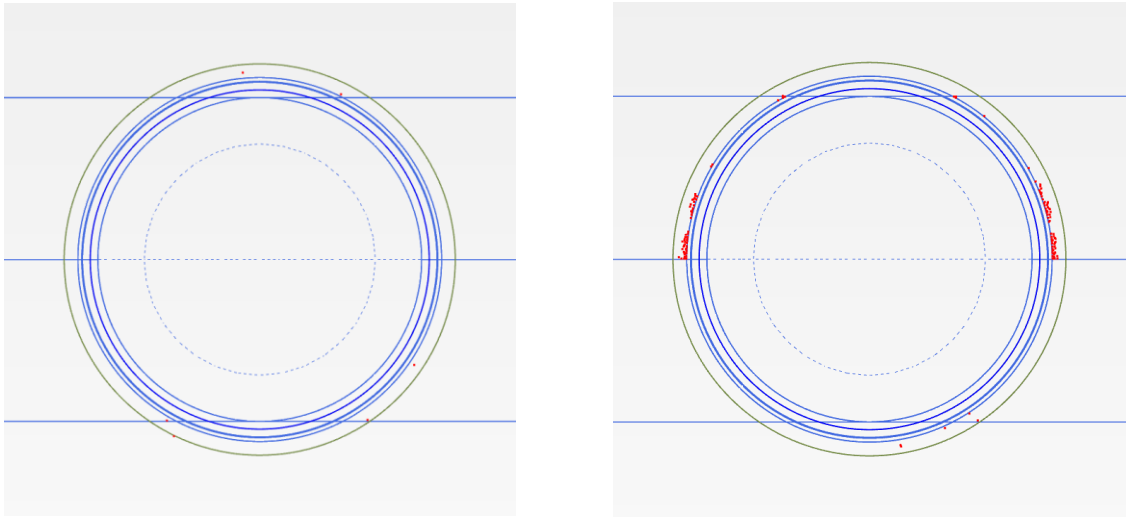

Fig. 60: Plastic points for the internal water pressure: Calculation 1 (left) and Calculation 2 (right).

Furthermore, the diametrical concrete and rock strains are evaluated according to Chapter 2.6.3.1 for both Calculation 1 and 2. The results are included in Table 15.

		Pressure: 11,1 bar		Release: 2,2 bar		Internal pres.: 5,5bar	
		ε_R	ε_c	ε_R	ε_c	ε_R	ε_c
On site		-0,43*10^{-4}	-3,36*10^{-4}	-0,10*10^{-4}	-0,67*10^{-4}	-0,26*10^{-4}	-0,50*10^{-4}
FE-Calculations	Mohr-Coulomb	-0,72*10^{-4}	-4,32*10^{-4}	-0,14*10^{-4}	-0,85*10^{-4}	-0,41*10^{-4}	-0,54*10^{-4}
	Calculation 1 $UCS_{Whirlpool}$ = 63 MPa	-0,68*10^{-4}	-4,31*10^{-4}	-0,14*10^{-4}	-0,85*10^{-4}	-0,40*10^{-4}	-0,56*10^{-4}
	Calculation 2 $UCS_{Whirlpool}$ = 0,3 MPa	-0,75*10^{-4}	-4,31*10^{-4}	-0,20*10^{-4}	-0,85*10^{-4}	-0,46*10^{-4}	-0,56*10^{-4}

Tab. 15: Comparison of the diametrical strains on site with the results of various calculations.

From Table 15 it can be concluded that the UCS reduction in Calculation 1 affects the rock and concrete strains to a marginal extent since the number of plastic points is small as illustrated in Figures 57 to 60.

The results of Calculation 2 demonstrate that a large reduction of the UCS is required to significantly affect the rock strains.

3 Summary

At the beginning the analytical solution for a circular ring under external pressure is used to calculate the normal force and the radial displacements of the tunnel lining.

The first calculations are performed for a constant pressure distribution along the tunnel perimeter using the MC-model. Therefore, two different calculation sections are analysed and the resulting normal force and displacements of the lining are compared with the analytical solution. During the investigations the significant influence of the gap stiffness on the actively applied pre-stressing pressure is pointed out by evaluating the normal force in the lining and the interface stresses for different values of E_{gap}.

Furthermore the diametrical displacements of the tunnel lining are evaluated according to the monitoring methods used on site.

In the next step the calculations are performed using an unsymmetrical pressure application along the tunnel perimeter. It is demonstrated that similar tunnel displacements as measured on site can be generated with an asymmetrically distributed pressure.

Further calculations are performed with the HB-material model and the results are compared with the MC-calculations. Different methods to fit the HB-failure line with equivalent MC-parameters are presented.

Finally, a Seeber-diagram based on the FE-results is developed and compared with the results obtained from the site.

4 Conclusions and outlook

From the comparison of the FE-results with the results of the analytical solution it can be concluded that the numerical modelling of pre-stressing pressure is possible.

The pressure application succeeds for a constant and unsymmetrical pressure distribution along the tunnel perimeter. In both cases the modelling of the gap stiffness plays a pivotal role for the resulting lining deformations.

Furthermore, the developed FE-model enables an estimation of the existing pre-stressing pressure along the tunnel perimeter on site.

From the Seeber-diagram based on the results of the FE-analysis it can be concluded that the partitioning of $\bar{p}_i$ during the watering-up matches with the results obtained from the site.

In Figure 54 it can be seen that the inclinations of the characteristic concrete and rock line developed on site deviate from the FE-calculations. A possible approach to reduce the divergence of the concrete lines is to model the final lining with 70cm instead of 60cm. Further investigations are necessary to determine the deviation of the characteristic rock lines.

5 List of references

[1] ILF: Design Report of the Niagara Tunnel Facility project. 25.05.2007

[2] Seeber, G.: Druckstollen und Druckschächte. Stuttgart: ENKE im Georg Thieme Verlag, 1999

[3] Vischer, D.; Huber, A.: Wasserbau. 5th circulation. Berlin: Springer, 1993

[4] Hoek, E.; Carranza-Torres, C.; Corkum, B.: Hoek-Brown failure criterion – 2002 edition. Proceedings of the North American Rock Mechanics Society Meeting. Toronto, 2002

[5] Hoek, E.; Brown, E.T.: Practical estimates of rock mass strength. Int. J. Rock. mech. Min. Sci., Vol. 34, No. 8, 1165-1186, 1997

[6] Nasekhian, A.: Application of Non- probabilistic and Probabilistic Concepts in Finite Element Analysis of Tunnelling. TU Graz, Dissertation, 2011

[7] Schubert, W.: Rock mechanics and tunneling. Lecture notes, 2010

6 List of tables

7 List of figures

8 Appendix

1. Longitudinal section
2. Typical cross section
3. Cross section for Calculation Section 1
4. Cross section for Calculation Section 2
5. MC- and HB-material parameters
6. Monitored lining deformations from the site
7. Excel sheet for diametrical concrete strain ε_c
8. Excel sheet for diametrical rock strain ε_R

GEOTECHNICAL LONGITUDINAL SECTION

SCALE 1:1000

STRATIGRAPHIC LEGEND FOR BOREHOLES

- OVERBURDEN
- GUELPH
- LOCKPORT (Eramosa)
- LOCKPORT (Goat Island)
- LOCKPORT (Gasport)
- DECEW
- ROCHESTER
- IRONDEQUOIT
- REYNALES
- NEAHGA
- THOROLD
- GRIMSBY
- POWERGLEN
- WHIRLPOOL

QUEENSTON FORMATION:

- V=MUDSTONE WITH COMPACTION FEATURES, SHEAR OR WEAK ZONE
- IV=REDDISH BROWN SILTY MUDSTONE
- IIIB=REDDISH BROWN MUDDY SILTSTONE WITH LESS THAN 40% GREEN MOTTLES
- IIIA=GREEN MUDDY SILTSTONE BAND OR GREATER THAN 40% GREEN
- IIB=INTERBEDDED SILTSTONE (LESS THAN 40% GREEN)
- IIA=INTERBEDDED SILTSTONE (GREATER THAN 40% GREEN)
- II=SILTSTONE
- NO CORE AVAILABLE
- FRACTURE FREQUENCY (FRACTURES/METRE)

FRACTURE ZONES

- F▷ FRACTURE
- C▶ CLAY
- L◀ CORE LOSS
- G— GOUGE
- S— UPPERMOST SILTSTONE BED LOGGED IN CORE

LEGEND:

CM...CONVERGENCE MONITORING SECTION

PI ...PIEZOMETER MONITORING SECTION

PIT...TUNNEL PIEZOMETER

EX ...EXTENSOMETER MONITORING SECTION

EL ...ELEVATION

1:1000 0 20 40 60 80 100 m

1:10000 0 200 400 600 800 1000 m

mf roll number	ver no	date	particulars	dwn / chkd	appd
	03	DEZ 07 2006	WATERPROOFING SYSTEM INCLUDED	MHA / PBO	
	02	AUG 24 2006	ISSUE FOR CONSTRUCTION	MHA / PBO	
	01	JUN 20 2006	FOR REVIEW OF 100% DESIGN	MHA / PBO	
	00	APR 03 2006	FOR REVIEW OF DESIGN BASIS	MHA / PBO	

NIAGARA TUNNEL FACILITY PROJECT

DIVERSION TUNNEL
GEOTECHNICAL LONGITUDINAL SECTION

ONTARIO POWER GENERATION

ILF BERATENDE INGENIEURE

STRABAG

dwn M. HABICHER | designed by P. BONAPACE
chkd P. BONAPACE
date yr/month/day 06/08/24 | design approved
scale 1:10000/1000 | authorized
plot scale 1:1 M | dist. code | CAD file type DWG
dwg no NAW130-DOV-29230-0016 | ver 03

A0 (841 x 1189) standard drawing number NAW130-DOV-29230-0016

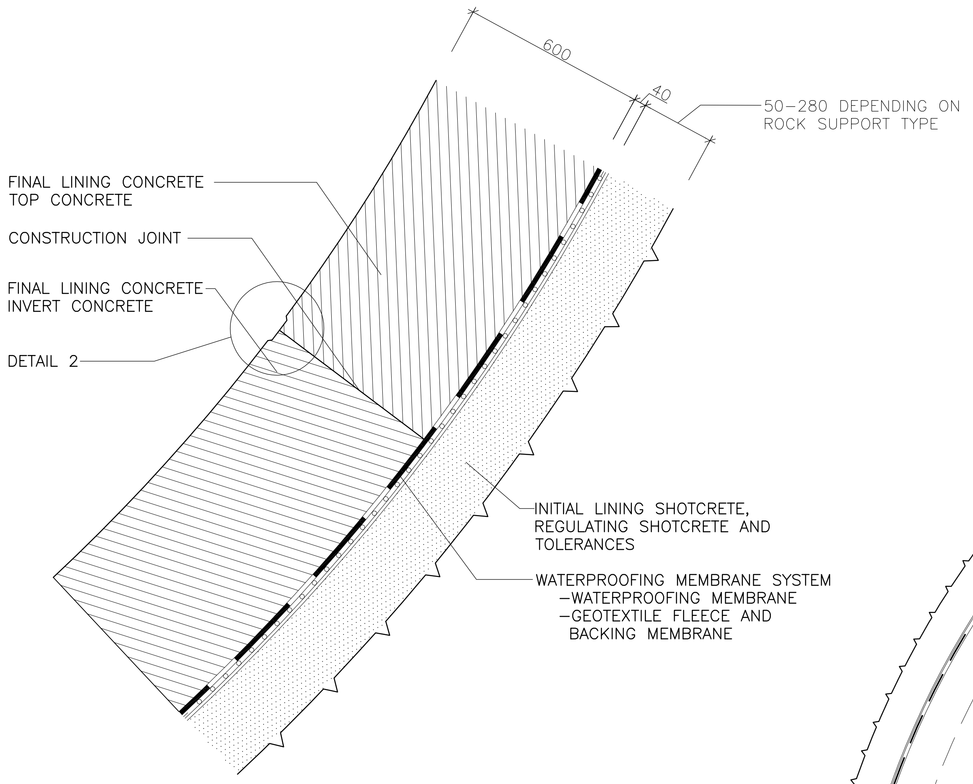

DETAIL – 1
SCALE: 1:10

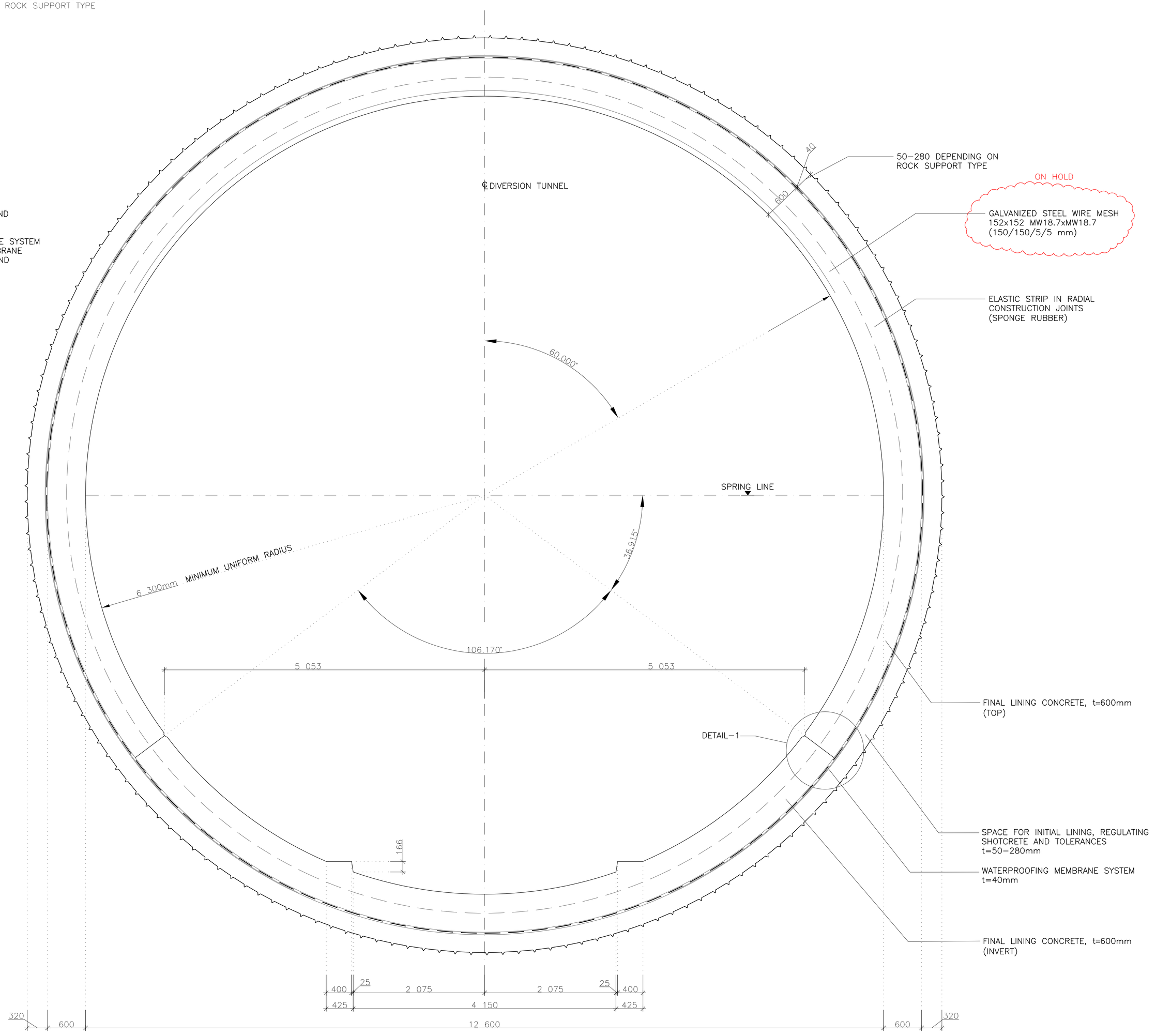

TYPICAL CROSS SECTION – 1, D_{TBM}=14.44m
SCALE 1:25

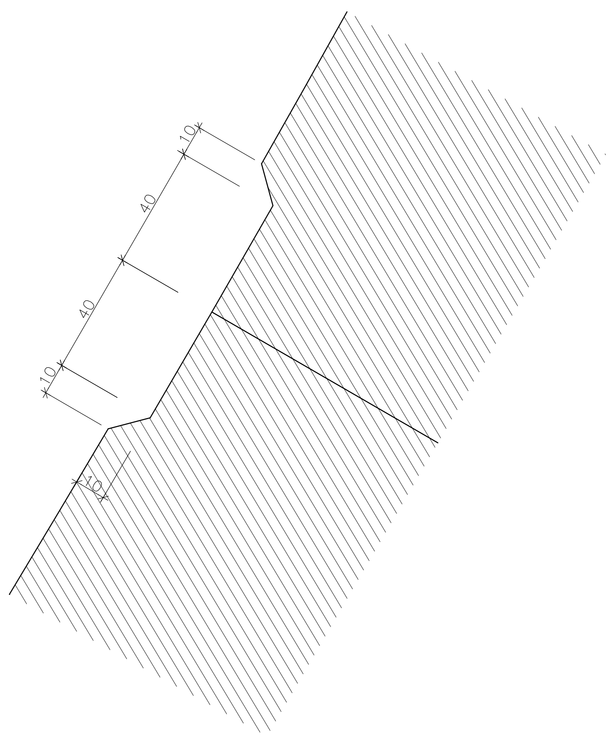

DETAIL – 2:
SCALE 1:1

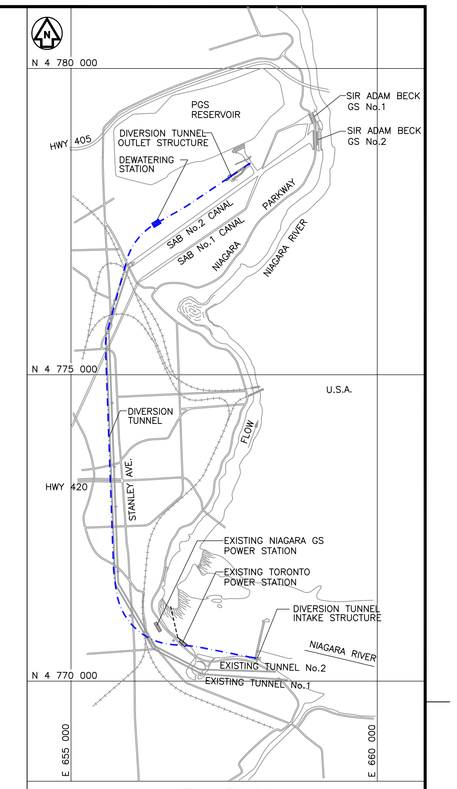

KEY PLAN
SCALE 1:50000

REFERENCE DRAWINGS:

NAW130–DOV–29230–0018
DIVERSION TUNNEL
ROCK SUPPORT TYPES 1 AND 2

NAW130–DOV–29230–0019
DIVERSION TUNNEL
ROCK SUPPORT TYPES 3 AND 4

NAW130–DOV–29230–0020
DIVERSION TUNNEL
ROCK SUPPORT TYPES 5 AND 6

MATERIALS:

FINAL LINING CONCRETE GRADE:
38MPa @ 90 DAYS, CYLINDER L:D=2:1

STEEL WIRE MESH GRADE: 400MPa

REGULATING SHOTCRETE GRADE:
25MPa @ 28 DAYS, CYLINDER L:D=1:1

WATERPROOFING MEMBRANE: TPO, FPO

GEOTEXTILE FLEECE: PP

BACKING MEMBRANE: PE

NOTES:

1. TOLERANCE ON INTERNAL RADIUS: ΔR=±50mm
2. INTERNAL RADIUS MAY BE ADJUSTED TO VARIABLE INITIAL LINING THICKNESS ACCORDING TO THE APPLIED TYPE OF ROCK SUPPORT
3. CONCRETE COVER TO INSIDE FACE: 75mm±20mm

1:1 0 20 40 60 80 100 mm
1:10 0 200 400 600 800 1000mm
1:25 0 0.5 1.0 1.5 2.0 2.5m

mf roll number	ver no	date	particulars	dwn / chkd	appd
	02	MAR 26 2007	ISSUE FOR CONSTRUCTION	MHA / PBO	
	01	OCT 17 2006	FOR REVIEW OF 100% DESIGN	MHA / PBO	
	00	JUN 20 2006	FOR REVIEW OF DESIGN BASIS	MHA / PBO	

NIAGARA TUNNEL FACILITY PROJECT

DIVERSION TUNNEL
TYPICAL CROSS SECTION
CH. 0+100 – CH. 10+388.274

ONTARIO POWER GENERATION

OLF BERATENDE INGENIEURE | STRABAG

dwn M. HABICHER	designed by P. BONAPACE		
chkd P. BONAPACE			
date yr/month/day 06/10/17	design approved	plot scale 1:1 M	
scale 1:25/1:10/1:1	authorized	CAD file type DWG	

dwg no NAW130–D0V–29230–0017 | ver 02

A0 (841 x 1189)
standard drawing number NAW130–D0V–29230–0017

0 10 50 100 200 250 300 millimetres

Calculation Section 1
km 1 + 411.000

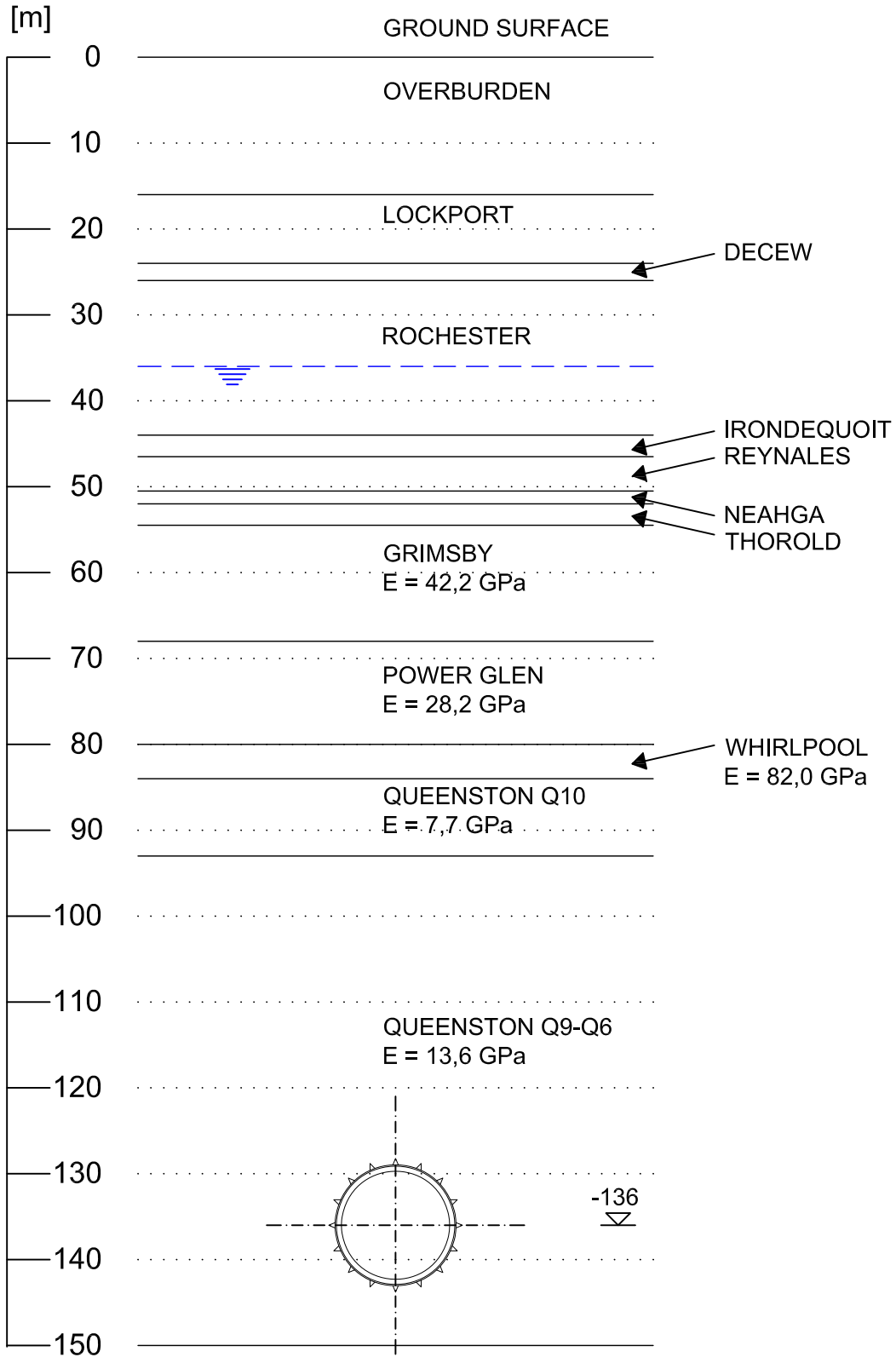

Calculation Section 2
km 0 + 726.939

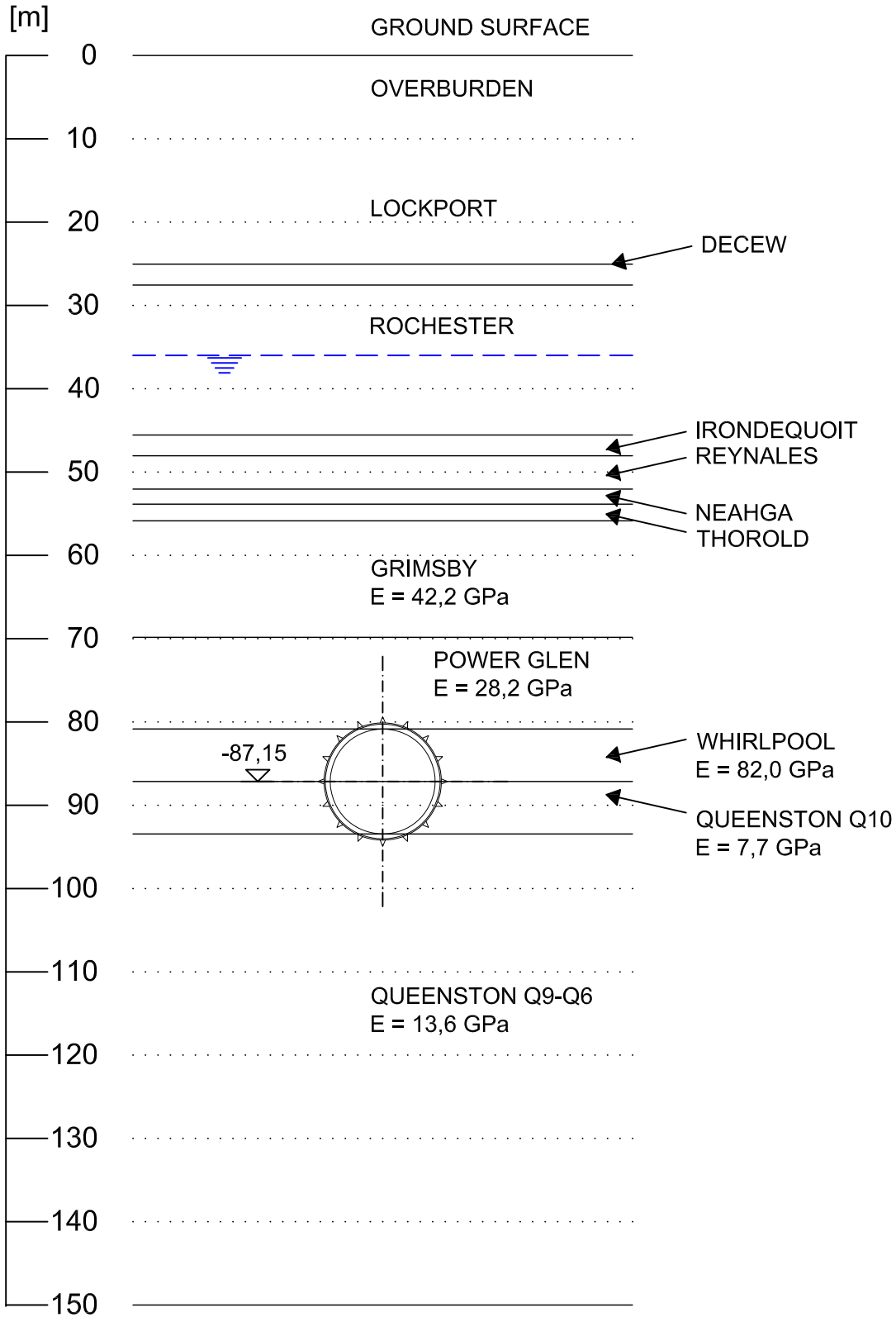

Diversion Tunnel - Design Report

Table A1: Evaluation of Rock Mass Parameters

Calculation section	Validity from	Validity to	Over-burden	Stress ratio	Groundwater above tunnel	Geological unit	UCS	GSI	mi	Minor principal effective stress	η			c			E		
[tunnel km]	[tunnel km]		[m]	η_H/η_V	[m]		[MPa]			[MPa]	[°]			[MPa]			[GPa]		
	(4)			(2)		(3)	(1)	(1)	(1)		(5)								
											mean	min	max	**mean**	min	max	**mean**	min	max
10+260	10+381	10+144	25	7.5	25	**Lockport/DeCew**	128	79	7	0.4	**53.2**	43.1	60.1	**6.9**	4.8	9.0	**53.1**	37.2	69.0
	0+072	0.000																	
9+950	10+144	9+844	45	7.5	45	**Rochester**	42	77	10	0.7	**55.0**	45.0	61.7	**1.7**	1.2	2.2	**30.7**	21.5	39.9
	0+272	0+072																	
9+580	9+844	9+293	60	7.5	60	**Irondequoit**	106	82	7	0.9	**51.0**	40.8	58.1	**6.9**	4.8	9.0	**63.1**	44.2	82.0
	0+700	0+272	65	7.5	65	**Reynales**	95	77	7	1.0	**52.1**	42.0	59.1	**4.5**	3.2	5.9	**46.1**	32.3	59.9
			65	7.5	65	**Nehaga**	14	66	10	1.0	**45.1**	35.1	52.5	**0.5**	0.3	0.6	**9.4**	6.6	12.2
			70	7.5	70	**Thorold**	163	83	15	1.1	**61.4**	52.1	67.2	**8.1**	5.7	10.5	**66.8**	46.8	86.8
			70	7.5	70	**Grimsby**	155	75	10	1.1	**57.7**	47.9	64.1	**5.5**	3.9	7.2	**42.2**	29.5	54.9
			70	7.5	70	**Grimsby Shale**	33	75	10	1.1	**51.9**	41.8	58.9	**1.3**	0.9	1.7	**24.2**	16.9	31.5
			85	7.5	85	**Powerglen**	172	68	10	1.3	**58.0**	48.2	64.3	**4.0**	2.8	5.2	**28.2**	19.7	36.7
			85	7.5	95	**Powerglen Shale**	24	68	10	1.3	**47.8**	37.7	55.1	**0.8**	0.6	1.0	**13.8**	9.7	17.9
			95	7.5	95	**Whirlpool**	216	87	15	1.4	**59.4**	49.8	65.5	**6.1**	4.3	7.9	**82.0**	57.4	106.6
8+666	9+293	7+505.5	130	4.5	100	**Queenston Q10**	33	55	6.5	2.3	**39.0**	29.5	46.5	**0.8**	0.6	1.0	**7.7**	5.4	10.0
	1+266	0+700																	
1+700	7+505.5	1+266	130	2.0	100	**Queenston Q9-Q6**	33	65	6.5	2.3	**41.4**	31.7	48.9	**1.1**	0.8	1.4	**13.6**	9.5	17.7
1+411			130	4.5	100	**Queenston Q9-Q6**	33	65	6.5	2.3	**41.4**	31.7	48.9	**1.1**	0.8	1.4	**13.6**	9.5	17.7

Remarks:

(1) Source: Design Build Agreement, Appendix 5.4 (GBR), Table 6.9.

(2) Stress ratios as given in Design Build Agreement, Appendix 5.4 (GBR), Chapter 6.6 and Table 6.14 are adopted in order to ensure stable initial conditions of the FE - analysis. (Levels rounded to 5 m)

(3) Boundary conditions (overburden and groundwater level) for Irondequoit, Reynales, Nehaga, Thorold, Grimsby, PowerGlen and Whirlpool are evaluated for the situation at the calculation section 9+580.

(4) The defined calculation sections are postulated to be valid for a certain sector of the tunnel (as indicated also in the Geotechnical Longitudinal Section.).

(5) The mean value is the 50% probability of occurrence average, and the range includes extreme values at 10% probability of occurrence that are 30% greater and 30% lower than the average. The range of the friction angle φ is defined on the basis of tan φ

NIAGARA TUNNEL FACILITY PROJECT

Review Deformation + Pre-stressing in Shift

Section 52

Background: STM based on vectors shown on vector plots, vector length used in direction of diagonal, all the time assumed tunnel is circle "not accured!!!"
MDM results from Laser 2 ist calculated as difference between (sum STM + MDM) - (STM before IG)

22.08.2011 **BAY STM 63** **IG Section 52** **TIME: 15:45** No pumps at works

	Point	1	2	3	4	5	6	7	8	Diameter	1-8	3-6	4-5	2-7	Δd max	Δd min	Oval [mm]		ΔD	ε_D
STM	Before IG [mm]	-0,38	0,5	-0,81	0,51	-0,37	0,34	-0,67	-0,06		-0,44	-0,47	0,14	-0,17	0,14	-0,47	0,61		-0,235	-1,8651E-05
	MDM S2 [mm]	-6,62	-5,60	-4,49	0,09	-3,43	0,96	-0,13	-1,34		-7,96	-3,53	-3,34	-5,73	-3,34	-7,96	4,62		-5,14	**-4,0794E-04**
	sum STM + MDM	-7,00	-5,10	-5,30	0,60	-3,80	1,30	-0,80	-1,40		-8,4	-4	-3,2	-5,9	-3,2	-8,4	5,2		-5,375	**-4,2659E-04**
		Radial Strain:				-2,69														

22.08.2011 **BAY STM 63** **IG Section 52** **TIME: 17;00**

	Point	1	2	3	4	5	6	7	8	Diameter	1-8	3-6	4-5	2-7	Δd max	Δd min	Oval [mm]		ΔD	ε_D
STM	Before IG [mm]	-0,38	0,5	-0,81	0,51	-0,37	0,34	-0,67	-0,06		-0,44	-0,47	0,14	-0,17	0,14	-0,47	0,61		-0,235	-1,8651E-05
	MDM S2 [mm]	-6,72	-5,80	-4,39	-0,01	-3,33	0,96	-0,13	-1,24		-7,96	-3,43	-3,34	-5,93	-3,34	-7,96	4,62		-5,165	**-4,0992E-04**
	sum STM + MDM	-7,10	-5,30	-5,20	0,50	-3,70	1,30	-0,80	-1,30		-8,4	-3,9	-3,2	-6,1	-3,2	-8,4	5,2		-5,4	**-4,2857E-04**
		Radial Strain:				-2,70														

22.08.2011 **BAY STM 63** **IG Section 52** **TIME: 19:19** No pumps at works

	Point	1	2	3	4	5	6	7	8	Diameter	1-8	3-6	4-5	2-7	Δd max	Δd min	Oval [mm]		ΔD	ε_D
STM	Before IG [mm]	-0,38	0,5	-0,81	0,51	-0,37	0,34	-0,67	-0,06		-0,44	-0,47	0,14	-0,17	0,14	-0,47	0,61		-0,235	-1,8651E-05
	MDM S2 [mm]	-7,22	-5,90	-4,99	0,29	-3,73	1,26	-0,53	-2,44		-9,66	-3,73	-3,44	-6,43	-3,44	-9,66	6,22		-5,815	**-4,6151E-04**
	sum STM + MDM	-7,60	-5,40	-5,80	0,80	-4,10	1,60	-1,20	-2,50		-10,1	-4,2	-3,3	-6,6	-3,3	-10,1	6,8		-6,05	**-4,8016E-04**
		Radial Strain:				-3,03														

22.08.2011 **BAY STM 63** **IG Section 52** **TIME:**

	Point	1	2	3	4	5	6	7	8	Diameter	1-8	3-6	4-5	2-7	Δd max	Δd min	Oval [mm]		ΔD	ε_D
STM	Before IG [mm]	-0,38	0,5	-0,81	0,51	-0,37	0,34	-0,67	-0,06		-0,44	-0,47	0,14	-0,17	0,14	-0,47	0,61		-0,235	-1,8651E-05
	MDM S2 [mm]	0,38	-0,50	0,81	-0,51	0,37	-0,34	0,67	0,06		0,44	0,47	-0,14	0,17	0,47	-0,14	0,61		0,235	**1,8651E-05**
	sum STM + MDM										0	0	0	0	0	0	0		0	**0,0000E+00**
		Radial Strain:				0,00														

Calculation of ε_c

Calculation Section 2: km 0 + 727

Calc. file in PLAXIS: Calc_0+727_MC_TP_3.4

Pressure admission: 11,1 bar constant

results for outer concrete strain

K0 = 1,5

			closest nodes in PLAXIS			Pressure phase			
								updated coordinates	
Monitoring points:	x [m]	y [m]	#	x [m]	y [m]	Pu_x [mm]	Pu_y [mm]	x [m]	y [m]
1	62,80648	51,30346	14778	62,81425	51,30000	-1,21399	-2,87683	62,81304	51,29712
2	57,19352	51,30346	12310	57,18575	51,30000	1,21400	-2,87683	57,18696	51,29712
3	66,37477	47,64052	19005	66,37477	47,64052	-2,75429	-1,30289	66,37202	47,63922
4	53,62523	47,64052	12620	53,62523	47,64052	2,75429	-1,30289	53,62798	47,63922
5	66,37477	42,35948	14540	66,37477	42,35948	-2,75265	0,97478	66,37202	42,36045
6	53,62523	42,35948	9563	53,62523	42,35948	2,75265	0,97478	53,62798	42,36045
7	62,80648	38,69654	12906	62,81425	38,70000	-1,21389	2,55028	62,81304	38,70255
8	57,19352	38,69654	10584	57,18575	38,70000	1,21389	2,55028	57,18696	38,70255

Initial diameter: 13800 mm

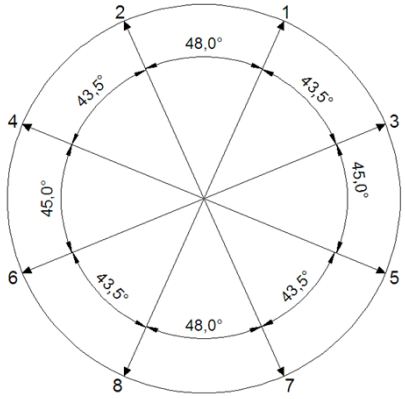

Pressure Phase [mm]			
D 1-8	D 3-6	D 4-5	D 2-7
13794,06	13794,05	13794,05	13794,06

ΔD [mm]				ØΔD	ε_D
D 1-8	D 3-6	D 4-5	D 2-7	[mm]	[-]
5,94	5,95	5,95	5,94	5,95	4,3112E-04

Calculation of ε_R

Calculation Section 2: km 0 + 727

Calc. file in PLAXIS Calc_0+727_MC_TP_3.4

Pressure admission: 11bar constant

results for rock strain

K0 = 1,5

			closest nodes in PLAXIS			Pressure phase		updated coordinates	
Monitoring points:	x [m]	y [m]	#	x [m]	y [m]	Pu_x [mm]	Pu_y [mm]	x [m]	y [m]
1	62,87000	51,46790	10235	62,89454	51,46127	0,13822	0,43452	62,89468	51,46170
2	57,12030	51,46790	7050	57,10546	51,46127	-0,13822	0,43451	57,10532	51,46170
3	66,54107	47,70940	17729	66,54107	47,70940	0,19421	0,27525	66,54126	47,70968
4	53,45893	47,70940	7486	53,45893	47,70940	-0,19422	0,27524	53,45874	47,70968
5	66,54107	42,29060	10166	66,54107	42,29060	0,61303	-0,25262	66,54168	42,29035
6	53,45893	42,29060	5738	53,45893	42,29060	-0,61304	-0,25261	53,45832	42,29035
7	62,87000	38,53210	8298	62,89454	38,53873	0,21410	-0,59651	62,89475	38,53813
8	57,12030	38,53210	5649	57,10546	38,53873	-0,21410	-0,59650	57,10525	38,53813

initial diameter: 14160 mm

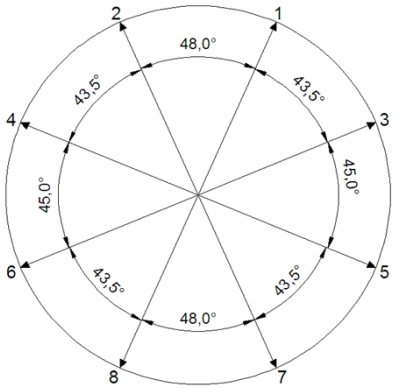

Pressure Phase [mm]			
D 1-8	D 3-6	D 4-5	D 2-7
14161,08	14160,95	14160,95	14161,08

ΔD [mm]				ØΔD	ε_D
D 1-8	D 3-6	D 4-5	D 2-7	[mm]	[-]
-1,08	-0,95	-0,95	-1,08	-1,02	-7,1863E-05